HHS Public Access

Author manuscript

J Chem Inf Model. Author manuscript; available in PMC 2024 July 10.

Published in final edited form as:

J Chem Inf Model. 2023 July 10; 63(13): 4190–4206. doi:10.1021/acs.jcim.3c00624.

Investigation of the Inhibition Mechanism of Xanthine Oxidoreductase by Oxipurinol: A Computational Study

Yazdan Maghsoud,

Department of Chemistry and Biochemistry, The University of Texas at Dallas, Richardson, Texas 75080, United States

Chao Dong,

Department of Chemistry and Physics, The University of Texas Permian Basin, Odessa, Texas 79762, United States

G. Andrés Cisneros

Department of Chemistry and Biochemistry and Department of Physics, The University of Texas at Dallas, Richardson, Texas 75080, United States

Abstract

Xanthine oxidoreductase (XOR) is an enzyme found in various organisms. It converts hypoxanthine to xanthine and urate, which are crucial steps in purine elimination in humans. Elevated uric acid levels can lead to conditions like gout and hyperuricemia. Therefore, there is significant interest in developing drugs that target XOR for treating these conditions and other diseases. Oxipurinol, an analogue of xanthine, is a well-known inhibitor of XOR. Crystallographic studies have revealed that oxipurinol directly binds to the molybdenum cofactor (MoCo) in XOR. However, the precise details of the inhibition mechanism are still unclear, which would be valuable for designing more effective drugs with similar inhibitory functions. In this study, molecular dynamics and quantum mechanics/molecular mechanics calculations are employed to investigate the inhibition mechanism of XOR by oxipurinol. The study examines the structural and dynamic effects of oxipurinol on the pre-catalytic structure of the metabolite-bound system. Our results provide insights on the reaction mechanism catalyzed by the MoCo center in the active site, which aligns well with experimental findings. Furthermore, the results provide insights

Corresponding Author: G. Andrés Cisneros – *Department of Chemistry and Biochemistry and Department of Physics, The University of Texas at Dallas, Richardson, Texas 75080, United States;* andres@utdallas.edu.

ASSOCIATED CONTENT

Supporting Information

The Supporting Information is available free of charge at https://pubs.acs.org/doi/10.1021/acs.jcim.3c00624.

Additional details of MD, EDA, NCI, and QM/MM (PDF)

Incorporation of the missing residues and construction of the initial model via the MODELER (ZIP)

Initial coordinates and parameters for the studied systems (ZIP)

Selected MD simulation representatives via the *k*-means clustering analysis for XO–OXI systems (ZIP)

Animation of the first principal modes, reaction paths, and the negative imaginary frequency for the approximate TS for each tautomer (ZIP)

Complete contact information is available at:
https://pubs.acs.org/10.1021/acs.jcim.3c00624

Notes

The authors declare no competing financial interest.

into the residues surrounding the active site and propose an alternative mechanism for developing alternative covalent inhibitors.

Graphical Abstract

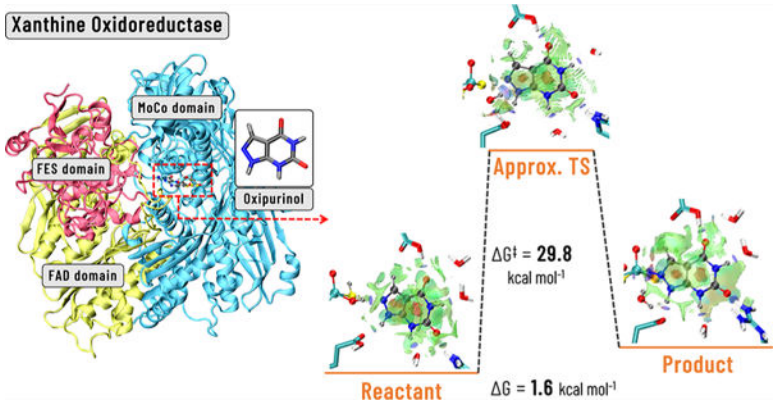

1. INTRODUCTION

Xanthine oxidoreductase (XOR) enzymes accelerate the hydroxylation of various substrates containing different functional groups such as aldehyde, purine, and pyrimidine. XOR proteins have been isolated from many organisms.[1–9] The active form of bovine XOR is a homodimer of molecular mass 290 kDa, where each subunit catalyzes the hydroxylation reaction independently.[10–12] As shown in Figure 1, each monomer has two iron–sulfur ($Fe_2 - S_2$ or FES) clusters, each bridged to four cysteine residues, one flavin adenine dinucleotide coenzyme (FAD), and one molybdopterin cofactor (MoCo). XOR proteins are highly homologous and consist of approximately 1330 amino acids. For example, the sequence identity between the bovine milk (1332 residues) and the human liver enzyme (1333 residues) is about 90%.[13,14] Proteolysis of mammalian XOR with trypsin and comparative sequence alignment indicated that the enzyme is divided into three fragments. The two FES clusters are located in the N-terminal fragment (20 kDa), the FAD is placed in the intermediate 40 kDa fragment, and the MoCo center is located in the C-terminal fragment with a molecular mass of 85 kDa.[15]

XOR is one of the most studied flavoproteins, and the redox reaction catalyzed in the heart of this enzyme is well established.[16–23] Mechanistically, the hydroxylation reaction occurs at the MoCo center of XOR and involves the reduction of Mo(VI) to Mo(IV).[10] After completing the reduction half-reaction at the MoCo, the electrons transfer via the FES clusters to the FAD cofactor to complete the oxidative half-reaction by the physiological electron acceptor, NAD^+ or O_2.[15]

Unlike other lower mammals such as cats and dogs, higher apes and humans lack a functional uricase gene that oxidizes urate into water-soluble allantoin.[24,25] Thus, uric acid is the final, irreversible product of purine breakdown by human XOR, which is excreted by the kidneys and intestinal tract, although it can be accumulated in the blood, leading to certain diseases.[26,27] Several clinical studies showed that hyperuricemia, the aftermath of

elevated levels of uric acid in serum, leads to gout and is associated with other medical conditions such as diabetes, cardiovascular disease, metabolic syndrome, and the formation of kidney stones.[28–36] Thus, uric acid excretion has to be increased, or its production by XOR needs to be reduced to decrease the blood concentration of uric acid and consequently treat these diseases.[37–40] The latter approach has been used to develop several drugs for this target.[40–46]

Allopurinol, an analogue of hypoxanthine, emerged as an effective inhibitor of xanthine oxidase (Scheme 1A, left).[48–50] Later, Massey et al.[51,52] realized that the active isomer, which effectively inhibits the XOR, is the hydroxylated form of allopurinol, i.e., oxipurinol (see Scheme 1A, middle). Oxipurinol has been considered the "gold standard" inhibitor of xanthine and has been widely prescribed ever since due to its excellent pharmacokinetic properties. However, the short dissociation half-life of 5 h[52] often leads to a high-dose prescription, rarely causing drastic side effects such as joint pain,[53] severe skin/mucous membrane rash (Steven–Johnson syndrome),[54,55] acute febrile neutrophilic dermatosis (Sweet's syndrome),[56] toxic epidermal necrolysis,[54,57] fulminant hepatitis,[58,59] and even renal failure in rare cases.[60,61] Due to these drawbacks, researchers worldwide have been designing more effective and longer-lasting inhibitors.[62–75] Among the proposed candidates, BOF-4272,[66,67,76] febuxostat,[69,77–79] piraxostat,[71,80,81] and topiroxostat[70,74,82–85] have been studied more extensively due to their promising inhibitory effects. Nevertheless, the search for new drugs continues[86–93] due to the increasing number of gout cases worldwide.[94–96]

The mechanism of the catalytic hydroxylation of XO's natural substrates, i.e., xanthine and hypoxanthine, and other purine- or non-purine-based inhibitors, has been extensively investigated by several experimental[97–105] and computational[106–115] studies. This mechanism involves a proton transfer from MoCo to E1261, as shown in Scheme 1B. Subsequently, the MoCo's negatively charged oxygen attacks the substrate's carbon adjacent to an N atom, with a transfer of "hydrogen and a negative charge" to the sulfido ligand (= S) and a concomitant reduction of the Mo cation from Mo(VI) to Mo(IV).[105,109,110,116] Afterward, the enzymatic turnover is completed by an incoming water molecule, leading to $2H^+$ and $2e^-$ release during the oxidation half-reaction.[117–119] It has been reported that the "hydrogen and a negative charge" transfer occurs in the form of a hydride ion.[10,23,109,110,116]

Quantum mechanics/molecular mechanics (QM/MM) studies by Cerqueira and co-workers[112] on the catalytic mechanism of XO with xanthine suggested that a hydrogen atom ($H^{\cdot}$) transfers to the sulfido group, while the second electron is transferred via the oxo-bridge. Hybrid spectroscopic/electronic structure studies by Kirk and co-workers[120,121] on purine-, non-purine, and aldehyde-based substrates also supported this mechanism. Our previous QM/MM study on the inhibition mechanism of the XO by topiroxostat and its hydroxylated metabolites (drug code: FYX-051) also suggested that the transferred hydrogen to the terminal sulfido at the transition state is nearly neutral and the other electron is transferred via the Mo–O–C bridge.[122]

As mentioned earlier, it had been envisaged that the allopurinol binds to the MoCo center in competition with xanthine. However, it eventually became clear that the inhibition is more

complicated and continues in a time-dependent manner, in which the allopurinol acts as a suicide inhibitor to produce oxipurinol.[52,98] Two crystallographic studies by Truglio et al.[47] and Nishino and co-workers[123] indicate that the reduced bovine milk XOR can be covalently bound to oxipurinol via the N8 atom of the substrate, which is a different coordination mode compared with other previously studied inhibitors (see Scheme 1A, middle). Another study by Nishino and co-workers[124] on the crystal structure of the reduced bovine milk XOR with trihydroxy-FYX-051 (the final hydroxylated metabolite of the topiroxostat family) showed similar coordination, in which the inhibitor is directly coordinated to the Mo atom via the nitrogen atom on the cyano group of the inhibitor (see Scheme 1A, right). Nishino and co-workers concluded that the nitrogen atom of the oxipurinol and the cyano nitrogen of trihydroxy-FYX-051 replace the water-exchangeable hydroxy ligand of the MoCo.

Allopurinol and topiroxostat (FYX-051) are two of the most clinically administered drugs for gout and hyperuricemia. In addition, the last metabolite of each drug forming the Mo−N complex has been identified as the inhibitor form that reduces uric acid levels in the body. Therefore, to develop more potent and efficient drugs with similar inhibition traits, it is crucial to gain a deeper understanding of the catalytic reaction mechanism involved in the last step of each drug. We extensively investigated the reaction mechanism of topiroxostat in our previous study, including its final metabolite.[122] Herein, we have studied the thermodynamics and kinetics of the inhibition reaction of XO by oxipurinol using classical molecular dynamics (MD) and QM/MM to determine the details of the reaction mechanism for the inhibition of XOR by this drug. The remainder of the paper is as follows; in the next section, we describe the approach for the MD and QM/MM simulations, including the structural, dynamical, binding affinity, and energy decomposition analyses, as well as the reaction path optimization and kinetic studies. Subsequently, the results are presented and discussed, followed by concluding remarks.

2. COMPUTATIONAL METHODS

The initial system was obtained based on the reduced bovine milk xanthine oxidoreductase bound to oxipurinol: PDB ID 3BDJ,[123] and all crystal waters were retained (resolution = 2.0 Å). The similarity between the human XOR[105,125] and the bovine isoform is around 90%. The employed PDB had missing fragments, including residues 1, 2, 165–192, 529–536, and 1318–1325, which comprise about 3% of the entire protein. Comparative modeling of XO's 3D structure and incorporation of the missing residues were performed using MODELER 10.1.[126,127] Further assessments were made by CASP[128] and CAMEO[129] to evaluate the accuracy of the constructed models. Finally, the best-suited modeled structure was selected for further MD simulations (see Figure S1).

The parameterization protocol applied for the FAD and FES cluster have been described previously.[122] However, the reduced form of MoCo and oxipurinol needed to be parameterized (see Figure S2). The AMBER force-field parameters calculated by Ramos and co-workers[130] were modified by the MCPB.py module[131] to obtain the parameters for the reduced MoCo (parameters provided in the Supporting Information), in which Mo(VI) is replaced by Mo(IV) and = S ligand is replaced by –SH (termed MoCo in the remainder of the paper). The oxipurinol substrate was parameterized via the R.E.D.

server[132–134] and ANTECHAMBER.[135,136] The protonation of all the amino acid residues was assessed via PROPKA.[137,138] Based on the findings by Truglio et al.[47] and Nishino and co-workers,[105,123,124] residues E802 and E1261 (key residues in the active site) are both protonated in the reduced XOR.

The LEaP module[139] of AMBER21[140] was used to construct the canonical structures of solvated apo-XO and XO–oxipurinol by adding hydrogen atoms, neutralizing the system with chloride counterions, and solvating the neutralized structure in a cubic box of TIP3P[141] water, extended at least 12 Å from the protein surface. The interactions between the atoms of the system were described with the protein's ff14SB[142] and general GAFF[135] force fields.

The pmemd.cuda module[143] of AMBER21 was utilized for conducting MD simulations. To perform minimization, positional restraints with a force constant of 100 kcal mol^{-1} $Å^{-2}$ were applied to all solute molecules. The minimization process consisted of 5000 cycles using the steepest descent method, followed by 5000 cycles with conjugate gradient. The system was subjected to further relaxation in seven steps, each consisting of 5000 MD steps with a time step of 1 fs with 100 kcal mol^{-1} $Å^{-2}$ restraint on the solute's heavy atoms. This process was conducted under constant pressure conditions, using the Berendsen barostat,[144] with the temperature maintained at 10 K. In the next step, each system was heated to 310 K using Langevin dynamics[145–147] with a collision frequency of 2 ps^{-1}, followed by 85 ns of NVT equilibration with decreasing restraint (50.0–0.0 kcal mol^{-1} $Å^{-2}$) on the protein's heavy atoms. Lastly, unrestrained NPT ensemble[145,147] simulations using a Langevin thermostat and Berendsen barostat[144,148] were carried out for 500 ns and 1 μs on three replicas, producing a total of 1.5 and 3.0 μs of simulation data for the apo-XO and XO–oxipurinol, respectively. Temperature was held constant at 310 K and pressure at 1.0 bar with a 2 fs time step. Long-range Coulomb interactions were approximated using the smooth particle mesh Ewald method,[143,149] and the van der Waals long-range interactions were approximated with the default isotropic correction implemented in AMBER using a 10 Å cutoff for non-bonded interactions. All bonds containing hydrogen atoms were treated with SHAKE[150] during the simulations.

The CPPTRAJ[151] module of AMBER21 was utilized for analyzing the production dynamics. Normal mode analysis was performed using the ProDy code.[152] Python libraries, namely, NumPy, Matplotlib, Pandas, and statsmodels module, along with the Gnuplot program were used for further data processing and two-dimensional plot graphing. MD simulations of replicates for each system were stable without significant fluctuations (see Figures S3–S11). The generated ensembles were used for clustering analysis. For the clustering analysis, 300,000 frames of the last 400 ns of all three replicates were subjected to a multi-dimensional analysis via the *k*-means algorithm,[153] as implemented in CPPTRAJ. The clustering dimensions corresponded to essential distances and angles between MoCo, oxipurinol, E802, and E1261. Initially, 30 representatives in ten clusters were obtained to identify the frames closest to each cluster's centroid. Later, eight representatives from the four clusters with the highest population abundance and the best orientations of the mentioned residues were selected for QM/MM optimizations (see Figures S12, S13, and Table S1).

Relative binding energies between oxipurinol and XO for two different tautomers were estimated using the MM/generalized Born surface area (GBSA) approach.[154–156] Calculations were carried out on the last 100,000 frames of each of the three replicates. A comprehensive explanation of the procedure utilized to compute the binding enthalpies had been previously provided.[122] The entropic contributions were not included in the calculations due to convergence issues; however, it has been shown that comparing the relative binding affinities of similar ligands via the MM/GB(*PB*)SA techniques can achieve satisfactory accuracy, even if the conformational entropy is neglected.[122,157–165]

QM/MM calculations were performed using LI-CHEM,[166,167] to interface Gaussian16[168] (for the QM region) and TINKER[169] (for the MM environment). The QM region was modeled using the ω B97X-D/def2-SVP[170,171] level of theory, while the MM environment was described using the AMBER ff14SB and TIP3P water force fields. The QM subsystem consists of 145 atoms, including the MoCo, oxipurinol, Q767, E802, R880, F914, F1009, E1261, and three water molecules that are placed within 3 Å of the substrate (see Figure S14). The remaining residues and solvent molecules within a 27 Å radius from the Mo center were described using the ff14SB and TIP3P potentials, respectively, while the rest were kept frozen. The reduced MoCo was tested for various multiplicities. Our calculations indicate that the most stable state corresponds to a singlet multiplicity, in agreement with Cerqueira and co-workers[112] and our previous study.[122]

After optimizing the chosen representatives, the reactant with the lowest QM/MM optimization energy was deemed the most stable, and the product was designed based on that structure. The resulting product structure was then subjected to QM/MM calculations using the same level of theory. The potential energy surface of the reaction path between the optimized reactant and product was obtained using the quadratic string method (QSM) combined with the restrained-MM optimization approach implemented in LI-CHEM.[167] Detailed explanations of the QM/MM calculation protocols can be found in our previous study.[122]

The reactants with the lowest QM/MM optimization energies were employed to calculate QM/MM interaction energies ($IE_{QM/MM}$) between the oxipurinol and XO via the following approach:[172]

$$IE_{QM/MM} = \left[QM^{\text{active site + OXI}} - (QM^{\text{active site}} + QM^{OXI})\right] + \left[MM^{OX-OXI} - MM^{\text{apoXO}}\right] \quad (1)$$

The terms $QM^{\text{active site + OXI}}$, $QM^{\text{active site}}$, and QM^{OXI} correspond to the single-point energies of the QM subsystem, the active site only (MoCo, Q767, E802, R880, F914, F1009, E1261, and $3H_2O$), and the tautomer of interest, respectively. The terms MM^{OX-OXI} and MM^{apoXO} correspond to the MM energies of the XO–OXI and apo-XO, respectively. The basis set superposition error (BSSE) correction is included in the $IE_{QM/MM}$ calculations using the counterpoise approach.[173,174]

The critical points were approximated by using the QM/MM-optimized structures and obtaining the frequencies and thermochemistry using only the electrostatically embedded system. These structures were subsequently used for vibrational analysis via Gaussian16[168] at the same levels of theory to calculate the approximate activation Gibbs free energies ($\Delta G^{\ddagger}$). One negative imaginary frequency was observed for the TS corresponding to the motion along the reaction coordinate (see animations in the Supporting Information). The Eyringpy[175,176] code was used to calculate the rate constant (k_{cat}) at 310 K based on the transition state theory (TST)[177,178] as

$$k = \sigma\kappa\frac{k_B T}{h}e^{-(\Delta G^{\ddagger})/RT} \quad (2)$$

where k_B and h are the Boltzmann and Planck constants, $\Delta G^{\ddagger}$ is the Gibbs free energy of activation of the studied reaction, σ is the reaction symmetry number which represents reaction path degeneracy, the number of different but equivalent reaction pathways that can be possible, and κ accounts for tunneling corrections which were calculated using the Eckart barrier approach[179] as implemented in the Eyringpy code.

Non-covalent index (NCI) analysis was performed to investigate non-covalent interaction (NCI) regions between oxipurinol and the binding pocket residues using the promolecular density method,[180] as implemented in the Multiwfn V. 3.8 program.[181] 5000 random snapshots from the last 100 ns of MD for the first replicate of each tautomer were used to analyze the electron density and its gradient norm during the dynamics, which allowed for the study of the averaged NCI (aNCI) regions. In addition, the QM/MM-optimized structures of the reactant, product, and the approximate TS were used to generate wavefunctions and calculate grid data of the reduced density gradient (RDG), which allowed for the study of the NCIs during the catalytic reaction. NCI surfaces were generated using the RGB color code to illustrate the strength of the interactions. Green and blue surfaces represented strong and weak interactions, such as hydrogen bonds and van der Waals (vdW) forces, while any repulsive interactions were depicted in red. The NCI surfaces were visualized with an isovalue of 0.4 a.u and a color scale of $-0.05\ \text{a.u.} < \text{sign}(\lambda_2)\rho < 0.05\ \text{a.u.}$

The QM/MM-optimized coordinates of the critical structures were also used to obtain all the wave functions for the electron localization function (ELF) analysis.[182] The ELF generates a scalar field that is both continuous and differentiable.[182,183] This field can be divided into basins, providing information on the classification of electron pairs within the system. A common notation is used to represent the basins associated with valence electrons, V(), which are associated with electron pairs belonging to one atom (monosynaptic basins, e.g., lone pairs), two atoms (disynaptic basins, e.g., covalent bonds), or three atoms (trisynaptic basins). The basin analysis[184,185] feature of Multiwfn V. 3.8[181] was employed to carry out the ELF calculations. The basin illustration was performed using a cubic grid of 200 a.u. with an isovalue of 0.8 a.u. and medium-quality grid with a spacing of 0.10 Bohr. Gaussian16[168] was used to generate the wave functions for the NCI and ELF calculations with Multiwfn and the cube files of the electrostatic potential (ESP) visualized with visual MD (VMD).[181,186] ESP charges were calculated using the Merz–Singh–Kollman scheme[187,188] implemented in Gaussian16.

Energy decomposition analysis (EDA) calculates the averaged energies of the non-bonded intermolecular interactions as a function of a reference residue(s). The nature of the intermolecular interactions between the protein and any fragment(s) of interest can be studied by this technique, which can be used to qualitatively assess the catalytic roles of individual amino acid residues.[122,172,189] Herein, an in-house Fortan90-based EDA code[190–192] was employed to study the intermolecular effects of the XO on the dynamics and kinetics of the inhibition by oxipurinol. To study the oxipurinol-bound pre-catalytic structure, EDA was run on 25,000 randomly selected snapshots of the 3 μs of the MD simulations from all three replicates. The total difference in the non-bonded intermolecular interaction energy between the MoCo and the protein environment during the MD simulation, ΔE_{NB}, can be calculated as

$$\Delta E_{\mathrm{NB}} = \langle E_{\mathrm{NB}} \rangle_{\mathrm{XO-OXI}} - \langle E_{\mathrm{NB}} \rangle_{\mathrm{apo-XO}} \quad (3)$$

where $\langle E_{\mathrm{NB}} \rangle_{\mathrm{XO-OXI}}$ and $\langle E_{\mathrm{NB}} \rangle_{\mathrm{apo-XO}}$ represent the average of non-bonded intermolecular interactions between the MoCo and each residue of the MM environment for the XO–oxipurinol and the apo-XO, respectively.

3. RESULTS AND DISCUSSION

3.1. Dynamics of the Pre-Catalytic Inhibition.

Xanthine and oxipurinol (also known as alloxanthine) are structurally related purine analogues that differ in the nature of their five-membered heterocyclic rings. Xanthine contains an imidazole ring, while oxipurinol features a pyrazole ring (see Scheme 1). Like xanthine, oxipurinol can exist as a mixture of tautomers (see Figure S15). Several reports on the chemical synthesis of oxipurinol have demonstrated that tautomer-1 represents the predominant tautomeric form of this compound.[48,193–198] In vitro and in vivo studies have also suggested that tautomer-1 is the functional derivative of oxipurinol with biological activity.[199–204] Moreover, Truglio et al.[47] suggested that the N9 nitrogen of oxipurinol (see Scheme 1A, middle) in their XDH–oxipurinol-inhibited crystal structure from *Rhodobacter capsulatus* (PDB ID: 1JRP) presumably acts as NH and forms a hydrogen bond to E730 (identical to E1261 in bovine XO). Hernández et al.[205] computationally showed that among the probable tautomers of oxipurinol, shown in Figure S15, di-keto tautomers (tautomers 1 and 2) are favorable in the gas phase and aqueous solution. In contrast, the keto–enol (tautomers 3–6) and di-enol (tautomers 7 and 8) forms are very unstable and largely disfavored. However, their results suggest that tautomer-1 is less favorable than tautomer-2 by ~3 kcal mol^{-1}.

It should be noted that experimental studies on allopurinol also show that the N9-protonated tautomer, shown in Scheme 1A-left, is the predominant form of neutral allopurinol.[206–208] In addition, another computational study by Hernandez et al.[194] on allopurinol showed that the N9-protonated tautomer of this inhibitor is the predominant form in both the gas phase and aqueous solution with the population of 99 and 88%, respectively. Given the collective findings, it is more likely that tautomer-1 is the principal inhibitor of xanthine oxidoreductase.

In our previous study on FYX-051 metabolites, we noticed that the incoming inhibitor exerts proximal and distal impacts on the movements of the enzyme.[122] It is observed in both the previous and the current study that the movements of the FES and FAD domains are non-correlated in the apo-XO (results are obtained from two different crystal structures), while the MoCo domain's movements are anti-correlated (see Figure 2A). Moreover, in our previous study, the inhibited enzyme's movements underwent significant changes following the binding of the inhibitor. Specifically, the MoCo domain displayed mostly correlated motions, whereas the other two domains exhibited varying movements in response to each metabolite. Herein, we aimed to investigate whether oxipurinol exhibits comparable effects on the enzyme movements and if there are any similarities between this inhibitor and trihydroxy-FYX-051, which has a similar mode of complexation to XO. Interestingly, similar to trihydroxy-FYX-051, the binding of oxipurinol results in a mostly non-correlated FES domain and completely anti-correlated FAD. Moreover, the residues of the MoCo domain remain correlated with MoCo, except for the areas adjacent to the FAD domain, which become non-correlated (Figure 2A). Taken together, our results indicate that ligand binding considerably affects the dynamics of the MoCo domain.

Root-mean-squared deviations (RMSDs) and atomic fluctuations for all the systems depicted in Figures S3–S8 show that significant movements primarily occur in the flexible loops of the protein's surface or on the modeled missing residues. The modeled residues were excluded from the principal component analysis (PCA); however, it is still evident that the largest PCA fluctuations are mainly centered around the removed residues and the flexible loops. The PCA results in Figures S3–S8 also indicate that the first two normal modes account for over 90% of the systems' movement modes in all structures. As the first normal mode makes up more than 75% of the movement modes for all structures, it was utilized to interpret the systems (refer to the animations in the Supporting Information). Figure 2A and the NMA animations in the Supporting Information also reveal that the directionality of the first normal mode's movements in the FES and FAD domains of apo-XO and XO–OXI are similar. Interestingly, the movements of the FES and FAD domains are smaller in magnitude for XO–OXI compared with that for apo-XO (see animations in the Supporting Information). The motion of the MoCo domain is similar between apo-XO and XO–OXI in some regions. Similar to the other two domains, the MoCo domain of apo-XO has larger movements than the inhibited-XO. Combining our observations with those of our previous investigation,[122] we suggest that oxipurinol, similar to trihydroxy-FYX-051, significantly enhances the stability of the MoCo domain.

Another helpful method for assessing the role of the enzyme's residues in the MoCo active site is to examine intermolecular interactions via an EDA. Here, we focused on a comparative investigation of the impact on the MoCo between the apo and inhibited structure to see whether oxipurinol stabilizes the MoCo domain. The difference of the non-bonded intermolecular interactions (ΔE_{NB}) between the protein and the MoCo was calculated with respect to apo-XO as the reference to study the intermolecular effects of oxipurinol (see Table S2). In addition, Figure 2B provides a three-dimensional illustration of the residues of the first, second, and third coordination shells that exhibit significant non-bonded interactions with the MoCo.

The calculated value of the sum of the individual calculated non-bonded interactions, $\sum \Delta E_{NB} \sim -174$ kcal mol^{-1}, suggests a strong attractive interaction between the protein and oxipurinol. Moreover, Table S2 shows that in addition to the MoCo domain's residues, several residues in the FES domain show significant stabilizing/destabilizing contributions to ΔE_{NB}. On the other hand, the FAD domain residues do not appear to have any substantial intermolecular interaction changes.

In our previous study, the stabilizing/destabilizing effects of several proximal and distal residues were observed during the inhibition reaction of XO by topiroxostat.[122] Besides, exhaustive studies on other metalloenzymes, such as human TET2 enzyme[209] and human histone demethylase,[210] have also identified the catalytic role of second coordination sphere (SCS) and long-range (LR) residues. Here, we were interested to see which residues around the active site considerably contribute to the reaction center of the oxipurinol-bound system consisting of MoCo, oxipurinol, and E1261—which are directly involved in the inhibition reaction. Calculated values of E_{NB} in Table S3 reveal several positively and negatively charged residues with $|E_{NB}| \geq 30$ kcal mol^{-1}, which respectively stabilize or destabilize the active site during the MD simulation. Figure 3A illustrates residues with significant intermolecular interactions that are located in the active site's first, second, and third coordination shells. As can be seen, several residues such as R829, R839, R871, R880, R899, K902, R912, K1045, K1052, S1080, R1134, K1250, and K1251 display significant stabilizing interactions with the active site, while negatively charged residues, D740, D745, D872, E879, E1037, D1084, E1092, E1196, E1209, and E1210, contribute to destabilization. Oxipurinol is predominantly surrounded by stabilizing contributors, among which R839 and R880 show substantial stabilizing effects ($E_{NB} \sim -61$ and -80 kcal mol^{-1}, respectively). In contrast, MoCo is mostly surrounded by destabilizing residues with only two residues, R912 and K1045, providing significantly large stabilizing interactions ($E_{NB} \sim -143$ and -105 kcal mol^{-1}, respectively).

A plot of the aNCIs along the dynamics simulation is shown in Figure 3B, illustrating the residues of the binding pocket having interacting surfaces with oxipurinol. Several binding pocket residues, including E802, R880, A910, F914, F1005, F1009, and E1261, show attractive interactions (in the NCI scale) with the inhibitor. Interestingly, in addition to R880 that exhibited a substantial stabilizing effect in our EDA analysis, all the other residues seen in the aNCI also have stabilizing contribution to the active site, especially E802 and F914 ($E_{NB} \sim -12$ and -11 kcal mol^{-1}, respectively). Taken together with the EDA, these results are consistent with an overall stabilizing environment of the protein in the binding pocket, promoting the binding of XO–OXI. Moreover, as shown in Figure 3A and Table S3, unprotonated aspartate and glutamate residues have destabilizing contributions to the MoCo active site. The stabilizing effect of the protonated E802 and its NCI with the inhibitor, which were also observed in our previous study on topiroxostat, agrees with the experimental results assuming the priority of protonated E802 over the negatively charged glutamate.[47,105,123,124]

As discussed in the beginning of this section, the di-keto isomer of oxipurinol is more stable than the other forms. Many studies have also supported that tautomer-1 (Figure S15)

is the primary product of synthesis and, thus, the active form of oxipurinol in inhibiting XOR. However, a computational study by Hernández et al.[205] has suggested tautomer-2 as a possible alternative. Therefore, this tautomeric form has also been studied here as a theoretically probable inhibitor, termed OXI^{T-2}, for the rest of the paper.

The binding affinities (ΔH_{bind}) between the inhibitor and the enzyme during the dynamics of the pre-catalytic reaction were calculated via the MM/GBSA approach (see Table S4). Calculated ΔH_{bind} values for the major (OXI) and the theoretical tautomer (OXI^{T-2}) are –24.5 and –25.8 kcal mol^{-1}, respectively, showing a slightly greater binding affinity for the later one. The QM/MM interaction energies ($IE_{QM/MM}$) between the inhibitor and the XO were also studied, which are –120.0 and –124.2 kcal mol^{-1}, respectively, showing a similar trend as the binding affinities. The components of the QM/MM interaction energies (Table S5, E_{QM} and E_{MM} of eq 1) suggest that despite the slight difference between $IE_{QM/MM}$ values, the differences between E_{QM} and E_{MM} for the tautomers are significant. The values of E_{QM} and E_{MM} for the major tautomer are similar (–58.9 and –61.1 kcal mol^{-1}, respectively), implying that its interaction with the enzyme is moderately stabilized by the active site (E_{QM}) and the solvated enzyme (E_{MM}). On the other hand, the E_{QM} value is more than twice that of E_{MM} for XO and the theoretical tautomer (–84.2 and –40.0 kcal mol^{-1}, respectively), suggesting that its interaction is mainly stabilized by the MoCo active site.

Taken together, the results of the binding affinities and interaction energies of these two forms propose the probability of a higher propensity of the theoretical tautomer to interact with the enzyme if presented in the active site.

3.2. Catalytic Inhibition Reaction.

Several studies have concluded that oxipurinol coordinates to the reduced MoCo during the enzymatic turnover.[52,124,211] However, extensive investigations by Spector and co-workers on both bovine and human xanthine oxidase provided particularly strong evidence that the reduced enzyme is susceptible to the inhibition by oxipurinol.[101,202,212,213] They realized that the enzyme undergoes inactivation when electron donors like xanthine and allopurinol substrates or the chemical reductant dithionite are present. In contrast, there is no inactivation in the absence of electron donors or when an artificial electron acceptor capable of directly re-oxidizing the MoCo is present. Moreover, Nishino and co-workers proposed that the XO–OXI complexation occurs in the presence of a proton.[124] Given that the XO–OXI complexation takes place during enzymatic turnover and a proton is required at the reaction center, which can be provided by E1261, a possible mechanism associated with this process, as depicted in Scheme 2, was investigated.

The proposed mechanism for oxipurinol is similar to the suggested mechanism for trihydroxy-FYX-051, in which the water-exchangeable hydroxyl ligand is replaced by the nitrogen atom to form a stable complex.[122] However, the pathway for the MoCo–OXI complexation involves the protonation of hydroxide ion (OH^-) by E1261, followed by the release of a water molecule (see animation in the Supporting Information). The resulting complex dissociates by a replacement of oxipurinol by an incoming water molecule,

resulting in the re-oxidation of the Mo to its original oxidation state, fulfilling the enzymatic turnover.

The results in Figure 4A suggest that the reaction is slightly endergonic ($\Delta E_{react} = 1.0$ kcal mol^{-1} and $\Delta G_{react} = 1.6$ kcal mol^{-1}). As shown in Figure 4C, the creation of V(Mo,N8) and V(O, Hε) ELF disynaptic basins in the product (bead 15) with electron populations of 3.1 e^- and 1.8 e^-, respectively, implies the formation of the MoCo–oxipurinol complex and a water molecule at this point (refer to Table S6 for the detailed values). The calculated energy barrier associated with the approximate TS (corresponding to bead 9) is 27.6(29.8) kcal mol^{-1}. At this point of the reaction mechanism, the Mo–OH bond cleaves, while the proton transfers from E1261 to the cleaving hydroxyl (Mo···OH···H···Glu), and the Mo···N8 bond forms between the MoCo and oxipurinol. The creation of ELF trisynaptic basins V(Mo,N8,C), V(Mo,O,H), and V-(O, Hε, Oε1) with electron populations of 2.7 e^-, 3.1 e^-, and 1.7 e^- at bead 9 also suggest the formation of the approximate TS at this point.

The QM/MM-optimized geometries of the key structures involved in the complexation reaction shown in Figure 4B provide calculated values for the product's O–Mo–N angle and Mo–N distance, which are 96° and 2.32 Å, respectively. These values are consistent with the experimental data from the referenced crystal structure with the reported values of 95° and 2.28 Å (see Scheme 1, middle). Moreover, the RMSD of the active site's atoms and the RMSD of the protein's backbone atoms with respect to the crystal structure are 1.3 and 3.1 Å, respectively. These distances, coupled with the blue surfaces of the NCIs in Figure 4A, suggest that oxipurinol maintains hydrogen bonds with N768, R880, E1261, and two water molecules along the catalytic reaction pathway. In addition, the blue NCI surfaces between the N8 nitrogen of oxipurinol and the hydrogen of MoCo's hydroxyl ligand in Figure 4A show a hydrogen bond between them. The presence of a hydrogen bond, combined with the cleavage of the hydroxyl ligand from the MoCo, may account for the relatively high barrier energy observed in both experiments and our calculations.

A larger view of the NCIs is provided in Figure S16 showing the NCIs between the binding pocket residues with the reactant and product. This figure highlights the important role of some residues such as E802, L873, R880, A910, F914, F1009, A1078, A1079, and E1261. In conjunction with the previous results of aNCI and EDA, residues R839, K902, F1005, S1080, and K1251 also play essential roles in the precatalytic and catalytic inhibition of XO by oxipurinol.

By examining the non-bonded contributions (EDA and NCI) to the MoCo's active site and comparing them to experimental mutagenesis studies on XO function, we can gain additional insights into the residues that significantly affect XO inhibition. As listed in Table S7, several studies have demonstrated that mutagenesis of E802,[105,214,215] R880,[105,216–219] and E1261,[105,217] which show substantial non-bonded interactions in our analyses, lead to complete loss of XO function. Our EDA and NCI results also show stabilizing effects by proximal residues such as G799, R912, and A1079, whose mutagenesis leads to partial or total loss of XO function.[218,220] Similar experimental effects were seen upon mutation of distal residues including R149,[221] H884,[218] and N887,[218] which are observed to have stabilizing effects from our present results. Moreover, several clinical trials on human

cases showed the substantial impact of residues R228,[222] R606,[223] K721,[224] R824,[219] and R1282[225] on lowering the XO activity (hypouricemia). Our EDA results show significant stabilizing effects of these residues on the active site. EDA results also suggest the destabilizing effects of residues I702, H1220, and T909 on the active site, suggesting that their mutation might promote the function of XO. Interestingly, clinical studies demonstrate the increasing activity of XO upon the mutation of these residues.[221,223] Overall, our results are consistent with experimental mutagenesis studies, and the predicted effects of residues within the binding pocket could be considered for developing analogues of oxipurinol with improved inhibitory effects.

The experimental activation energy values for the XO inactivation ($\Delta G^{\ddagger}_{\text{inact}}$) by oxipurinol are 31 and 28 kcal mol^{-1} for human and bovine xanthine oxidase, respectively,[101] which are in good agreement with our calculated barrier free energy in Figure 4A ($\Delta G^{\ddagger}$= 29.8 kcal mol^{-1}). The corresponding corrected rate constant (k_{cat}) calculated via the results of the vibrational analysis is 3.4×10^{-9} s^{-1}.

Several studies have indicated that oxipurinol-inactivated XO can be reactivated at varying rates. The slowest reactivation rate is through spontaneous means.[50,52] Cycling of the enzyme in the presence of the xanthine substrate leads to an intermediate reactivation rate,[212] while re-oxidizing the reduced MoCo via artificial electron acceptors results in a quick reactivation.[52,226,227] The experimental activation energy values for the spontaneous reactivation process ($\Delta G^{\ddagger}_{\text{react}}$) are 25 and 27 kcal mol^{-1} for human and bovine XO, respectively.[101] These values are in good agreement with our calculated backward barrier corresponding to 26.6(28.2) kcal mol^{-1}. Notably, the calculated backward barrier ($\Delta E^{\ddagger}_{\text{backward}}$) for trihydroxy-FYX-051 in our previous study[122] was 32.6 kcal mol^{-1}, which is ~6–7 kcal mol^{-1} larger than that calculated for oxipurinol. This difference in backward barriers may (at least partially) help explain the observed differences in dissociation half-lives ($t_{1/2}$) between oxipurinol (~5 h)[52] and trihydroxy-FYX-051 (~20.4 to 72 h).[74]

As mentioned before, OXI$^{\text{Tn}-2}$ was also considered a possible theoretical alternative for the biologically active tautomer. The proposed mechanism for this form and the corresponding reaction path study are provided in Section 13 of the Supporting Information (Figures S17–S20). Interestingly, the inhibition reaction by this form, which involves a spontaneous proton transfer from the tautomer to the hydroxyl ligand of MoCo, is −10.7 kcal mol^{-1}, and the energy barrier is 14.8 kcal mol^{-1}. These results suggest that the catalytic inhibition might be more favorable for this tautomer if this molecule (or a similar analogue) could be synthesized. This might suggest possible routes for designing new analogues of oxipurinol with a similar coordination mode to this tautomeric form.

Taken together, our results align with experimental reports for the functional derivative of oxipurinol that possesses XO-inhibiting activity. However, the thermodynamics and kinetics of the catalytic reactions propose that cleavage of the water ligand might be more favorable than the hydroxy ligand. This suggests that similar candidates with accessible proton (e.g., −NH instead of −N) might facilitate the ligand exchange and consequently the XO–inhibitor complexation. Furthermore, the observation of stabilizing the active site's environment

upon the binding of oxipurinol underscores the important contribution of multiple residues surrounding the binding cavity as non-covalent interacting partners. In designing new candidate inhibitors, these amino acids can serve as targets for NCIs.

4. CONCLUSIONS

Oxipurinol, the active metabolite of allopurinol, is widely used to treat gout and hyperuricemia as an effective xanthine oxidase inhibitor. However, its inhibition mechanism has not been studied at the atomic level. The MD results show proximal stabilizing effects of the incoming inhibitors on the active site's environment and distal influences on the MoCo, FES, and FAD domains. EDA results suggest several residues located in the first, second, and third coordination shells of the active site with substantial stabilizing effects such as E802, R880, R912, F914, S1080, and K1045. In addition, oxipurinol forms NCIs with E802, L873, R880, A910, F914, F1005, F1009, A1078, A1079, and E1261 during the pre-catalytic and catalytic stages of the inhibition. A probable inhibition mechanism was investigated based on the insights provided by previous experimental studies, which turned out to be thermodynamically feasible compared to the experimental observations. The product state for XO–OXI is endergonic with a calculated reaction energy of 1.0 kcal mol^{-1}. The proximity between the experimental activation energy for the enzyme inactivation by oxipurinol ($\Delta G^{\ddagger}_{inact}$= 28 kcal mol^{-1} for bovine XO) with the calculated energy barrier ($\Delta G^{\ddagger} \sim 29.8$ kcal mol^{-1}) suggests that our proposed mechanism may be kinetically feasible. Moreover, our calculated backward barrier is 26.6 kcal mol^{-1}, consistent with the experimental activation energy values for the spontaneous reactivation process ($\Delta G^{\ddagger}_{react}$= 27 kcal mol^{-1} for bovine XO). Calculated intermolecular interaction results underscore the important role of several residues during the enzyme inhibition process, including E802, L873, R880, A910, F914, F1005, F1009, A1078, A1079, S1080, and E1261, which could be considered as significantly interacting residues that may be exploited for the future development of more potent oxipurinol analogues.

Supplementary Material

Refer to Web version on PubMed Central for supplementary material.

ACKNOWLEDGMENTS

This study is funded by NIH Grant No. R01GM108583. MD simulations for this project were performed on the Ganymede2 and Titan HPC clusters at the University of Texas at Dallas' Cyberinfrastructure and Research Services. The QM/MM calculations were implemented on the CASCaM CRUNTCh3 and CRUNTCh4 HPC clusters at the University of North Texas' Chemistry Department, partially funded by the NSF Grant Nos. CHE1531468 and OAC-2117247. The authors thank Professors Filippo Romiti and Michael Biewer for insightful discussions.

Data Availability Statement

All simulations and analyses employed via third-party software are described and referenced in the Computational Methods section. The EDA and LICHEM software programs are available at the Cisneros Research Group GitHub: https://github.com/CisnerosResearch/AMBER-EDA and https://github.com/CisnerosResearch/LICHEM.

REFERENCES

1. Pritsos CA Cellular distribution, metabolism and regulation of the xanthine oxidoreductase enzyme system. Chem.-Biol. Interact 2000, 129, 195–208. [PubMed: 11154741]
2. Garattini E; Mendel R, Romão MJ, Wright R, Terao M Mammalian molybdo-flavoenzymes, an expanding family of proteins: structure, genetics, regulation, function and pathophysiology. Biochem. J 2003, 372, 15–32. [PubMed: 12578558]
3. Hesberg C; Hansch R; Mendel RR; Bittner F Tandem Arabidopsis thaliana: differential gene expression and enzyme activities. J. Biol. Chem 2004, 279, 13547–13554. [PubMed: 14726515]
4. Yasuhara A; Akiba-Goto M; Aisaka K Cloning and sequencing of the aldehyde oxidase gene from Methylobacillus sp. KY4400. Biosci., Biotechnol., Biochem 2005, 69, 2435–2438. [PubMed: 16377905]
5. Mendel RR Biology of the molybdenum cofactor. J. Exp. Bot 2007, 58, 2289–2296. [PubMed: 17351249]
6. Zhang Y; Gladyshev VN Molybdoproteomes and evolution of molybdenum utilization. J. Mol. Biol 2008, 379, 881–899. [PubMed: 18485362]
7. Kurosaki M; Bolis M; Fratelli M; Barzago MM; Pattini L; Perretta G; Terao M; Garattini E Structure and evolution of vertebrate aldehyde oxidases: from gene duplication to gene suppression. Cell. Mol. Life Sci 2013, 70, 1807–1830. [PubMed: 23263164]
8. Garattini E; Terao M Aldehyde oxidase and its importance in novel drug discovery: present and future challenges. Expert Opin. Drug Discovery 2013, 8, 641–654.
9. Marelja Z; Dambowsky M; Bolis M; Georgiou ML; Garattini E; Missirlis F; Leimkühler, S. The four aldehyde oxidases of Drosophila melanogaster have different gene expression patterns and enzyme substrate specificities. J. Exp. Biol 2014, 217, 2201–2211. [PubMed: 24737760]
10. Rajagopalan K; Johnson JL The pterin molybdenum cofactors. J. Biol. Chem 1992, 267, 10199–10202. [PubMed: 1587808]
11. Romão MJ Archer M; Moura I; Moura JJ; LeGall J; Engh R; Schneider M; Hof P; Huber R Crystal structure of the xanthine oxidase-related aldehyde oxido-reductase from D. gigas. Science 1995, 270, 1170–1176. [PubMed: 7502041]
12. Xia M; Dempski R; Hille R The reductive half-reaction of xanthine oxidase: reaction with aldehyde substrates and identification of the catalytically labile oxygen. J. Biol. Chem 1999, 274, 3323–3330. [PubMed: 9920873]
13. Kimiyoshi I; Yoshihiro A; Kumi N; Shinsei M; Tatsuo H; Osamu S; Nobuyoshi S; Takeshi N Cloning of the cDNA encoding human xanthine dehydrogenase (oxidase): structural analysis of the protein and chromosomal location of the gene. Gene 1993, 133, 279–284. [PubMed: 8224915]
14. Berglund L; Rasmussen J; Andersen M; Rasmussen M; Petersen T Purification of the bovine xanthine oxidoreductase from milk fat globule membranes and cloning of complementary deoxyribonucleic acid. J. Dairy Sci 1996, 79, 198–204. [PubMed: 8708081]
15. Hille R; Nishino T Xanthine oxidase and xanthine dehydrogenase. FASEB J 1995, 9, 995–1003. [PubMed: 7649415]
16. Harrison R Structure and function of xanthine oxidoreductase: where are we now? Free Radical Biol. Med 2002, 33, 774–797. [PubMed: 12208366]
17. Berry CE; Hare JM Xanthine oxidoreductase and cardiovascular disease: molecular mechanisms and pathophysiological implications. J. Physiol 2004, 555, 589–606. [PubMed: 14694147]
18. Alderman M; Aiyer KJ Uric acid: role in cardiovascular disease and effects of losartan. Curr. Med. Res. Opin 2004, 20, 369–379. [PubMed: 15025846]
19. Hille R Molybdenum-containing hydroxylases. Arch. Biochem. Biophys 2005, 433, 107–116. [PubMed: 15581570]
20. Nishino T; Okamoto K; Eger BT; Pai EF; Nishino T Mammalian xanthine oxidoreductase−mechanism of transition from xanthine dehydrogenase to xanthine oxidase. FEBS J 2008, 275, 3278–3289. [PubMed: 18513323]
21. Nossaman VE; Nossaman BD; Kadowitz PJ Nitrates and nitrites in the treatment of ischemic cardiac disease. Cardiol. Rev 2010, 18, 190. [PubMed: 20539102]

22. Agarwal A; Banerjee A; Banerjee U Xanthine oxidoreductase: a journey from purine metabolism to cardiovascular excitation-contraction coupling. Crit. Rev. Biotechnol 2011, 31, 264–280. [PubMed: 21774633]
23. Hille R; Nishino T; Bittner F Molybdenum enzymes in higher organisms. Coord. Chem. Rev 2011, 255, 1179–1205. [PubMed: 21516203]
24. Folin O; Berglund H; Derick C The uric acid problem. An experimental study on animals and man, including gouty subjects. J. Biol. Chem 1924, 60, 361.
25. Shestopalov A; Shkurat T; Mikashinovich Z; Kryzhanovskaya I; Bogacheva M; Lomteva S; Prokof'Ev V; Gus'Kov E Biological functions of allantoin. Biol. Bull 2006, 33, 437–440.
26. Kelley EE; Khoo NK; Hundley NJ; Malik UZ; Freeman BA; Tarpey MM Hydrogen peroxide is the major oxidant product of xanthine oxidase. Free Radical Biol. Med 2010, 48, 493–498. [PubMed: 19941951]
27. Flemmig J; Kuchta K; Arnhold J; Rauwald H Olea europaea leaf (Ph. Eur.) extract as well as several of its isolated phenolics inhibit the gout-related enzyme xanthine oxidase. Phytomedicine 2011, 18, 561–566. [PubMed: 21144719]
28. Obermayr RP; Temml C; Gutjahr G; Knechtelsdorfer M; Oberbauer R; Klauser-Braun R Elevated uric acid increases the risk for kidney disease. J. Am. Soc. Nephrol 2008, 19, 2407–2413. [PubMed: 18799720]
29. Kanbay M; Segal M; Afsar B; Kang D-H; Rodriguez-Iturbe B; Johnson RJ The role of uric acid in the pathogenesis of human cardiovascular disease. Heart 2013, 99, 759–766. [PubMed: 23343689]
30. Li C; Hsieh M-C; Chang S-J Metabolic syndrome, diabetes, and hyperuricemia. Curr. Opin. Rheumatol 2013, 25, 210–216. [PubMed: 23370374]
31. Jalal DI Hyperuricemia, the kidneys, and the spectrum of associated diseases: a narrative review. Curr. Med. Res. Opin 2016, 32, 1863–1869. [PubMed: 27470664]
32. El Din UAS; Salem MM; Abdulazim DO Uric acid in the pathogenesis of metabolic, renal, and cardiovascular diseases: A review. J. Adv. Res 2017, 8, 537–548. [PubMed: 28748119]
33. Kuwabara M; Niwa K; Nishihara S; Nishi Y; Takahashi O; Kario K; Yamamoto K; Yamashita T; Hisatome I Hyperuricemia is an independent competing risk factor for atrial fibrillation. Int. J. Cardiol 2017, 231, 137–142. [PubMed: 27871785]
34. Johnson RJ; Bakris GL; Borghi C; Chonchol MB; Feldman D; Lanaspa MA; Merriman TR; Moe OW; Mount DB; Lozada LGS Hyperuricemia, acute and chronic kidney disease, hypertension, and cardiovascular disease: report of a scientific workshop organized by the National Kidney Foundation. Am. J. Kidney Dis 2018, 71, 851–865. [PubMed: 29496260]
35. Borghi C; Agabiti-Rosei E; Johnson RJ; Kielstein JT; Lurbe E; Mancia G; Redon J; Stack AG; Tsioufis KP Hyperuricaemia and gout in cardiovascular, metabolic and kidney disease. Eur. J. Intern. Med 2020, 80, 1–11. [PubMed: 32739239]
36. Nishikawa T; Nagata N; Shimakami T; Shirakura T; Matsui C; Ni Y; Zhuge F; Xu L; Chen G; Nagashimada M Xanthine oxidase inhibition attenuates insulin resistance and dietinduced steatohepatitis in mice. Sci. Rep 2020, 10, 815. [PubMed: 31965018]
37. Khanna D; Fitzgerald JD; Khanna PP; Bae S; Singh MK; Neogi T; Pillinger MH; Merill J; Lee S; Prakash S American College of Rheumatology guidelines for management of gout. Part 1: systematic nonpharmacologic and pharmacologic therapeutic approaches to hyperuricemia. Arthritis Care Res 2012, 64, 1431–1446, DOI: 10.1002/acr.21772.
38. Khanna D; Khanna PP; Fitzgerald JD; Singh MK; Bae S; Neogi T; Pillinger MH; Merill J; Lee S; Prakash S American College of Rheumatology guidelines for management of gout. Part 2: therapy and antiinflammatory prophylaxis of acute gouty arthritis. Arthritis Care Res 2012, 64, 1447–1461.
39. Miner JN; Tan PK; Hyndman D; Liu S; Iverson C; Nanavati P; Hagerty DT; Manhard K; Shen Z; Girardet J-L Lesinurad, a novel, oral compound for gout, acts to decrease serum uric acid through inhibition of urate transporters in the kidney. Arthritis Res. Ther 2016, 18, 124. [PubMed: 27255643]
40. Tan PK; Liu S; Gunic E; Miner JN Discovery and characterization of verinurad, a potent and specific inhibitor of URAT1 for the treatment of hyperuricemia and gout. Sci. Rep 2017, 7, 665. [PubMed: 28386072]

41. Nguyen MTT; Awale S; Tezuka Y; Le Tran Q; Kadota S Xanthine oxidase inhibitors from the heartwood of Vietnamese Caesalpinia sappan. Chem. Pharm. Bull 2005, 53, 984–988.
42. Higgins P; Ferguson LD; Walters MR Xanthine oxidase inhibition for the treatment of stroke disease: a novel therapeutic approach. Expert Rev. Cardiovasc. Ther 2011, 9, 399–401. [PubMed: 21517722]
43. Harrold L New developments in gout. Curr. Opin. Rheumatol 2013, 25, 304–309. [PubMed: 23466959]
44. Gliozzi M; Malara N; Muscoli S; Mollace V The treatment of hyperuricemia. Int. J. Cardiol 2016, 213, 23–27. [PubMed: 26320372]
45. Yu W; Cheng J-D Uric acid and cardiovascular disease: an update from molecular mechanism to clinical perspective. Front. Pharmacol 2020, 11, No. 582680. [PubMed: 33304270]
46. Yu Z; Kan R; Wu S; Guo H; Zhao W; Ding L; Zheng F; Liu J Xanthine oxidase inhibitory peptides derived from tuna protein: virtual screening, inhibitory activity, and molecular mechanisms. J. Sci. Food Agric 2021, 101, 1349–1354. [PubMed: 32820534]
47. Truglio JJ; Theis K; Leimkühler S; Rappa R; Rajagopalan K; Kisker C Crystal structures of the active and alloxanthineinhibited forms of xanthine dehydrogenase from Rhodobacter capsulatus. Structure 2002, 10, 115–125. [PubMed: 11796116]
48. Robins RK Potential purine antagonists. I. Synthesis of some 4, 6-substituted pyrazolo [3, 4-d] pyrimidines1. J. Am. Chem. Soc 1956, 78, 784–790.
49. Elion GB; Callahan S; Nathan H; Bieber S; Rundles RW; Hitchings GH Potentiation by inhibition of drug degradation: 6-substituted purines and xanthine oxidase. Biochem. Pharmacol 1963, 12, 85–93.
50. Elion GB Enzymatic and metabolic studies with allopurinol. Ann. Rheum. Dis 1966, 25, 608. [PubMed: 5958693]
51. Massey V; Brumby PE; Komai H; Palmer G Studies on milk xanthine oxidase: some spectral and kinetic properties. J. Biol. Chem 1969, 244, 1682–1691. [PubMed: 5813728]
52. Massey V; Komai H; Palmer G; Elion GB On the mechanism of inactivation of xanthine oxidase by allopurinol and other pyrazolo [3, 4-d] pyrimidines. J. Biol. Chem 1970, 245, 2837–2844. [PubMed: 5467924]
53. Hill EM; Sky K; Sit M; Collamer A; Higgs J Does starting allopurinol prolong acute treated gout? A randomized clinical trial. J. Clin. Rheumatol 2015, 21, 120–125. [PubMed: 25807090]
54. Hasegawa A; Abe R Recent advances in managing and understanding Stevens-Johnson syndrome and toxic epidermal necrolysis. F1000Res 2020, 9, 612.
55. Halevy S; Ghislain P-D; Mockenhaupt M; Fagot J-P; Bavinck JNB; Sidoroff A; Naldi L; Dunant A; Viboud C; Roujeau J-C Allopurinol is the most common cause of Stevens-Johnson syndrome and toxic epidermal necrolysis in Europe and Israel. J. Am. Acad. Dermatol 2008, 58, 25–32. [PubMed: 17919772]
56. Polimeni G; Cardillo R; Garaffo E; Giardina C; Macri R; Sirna V; Guarneri C; Arcoraci V Allopurinol-induced Sweet's syndrome. Int. J. Immunopathol. Pharmacol 2016, 29, 329–332. [PubMed: 26684631]
57. Scavone C; Di Mauro C; Ruggiero R; Bernardi FF; Trama U; Aiezza ML; Rafaniello C; Capuano A Severe cutaneous adverse drug reactions associated with allopurinol: an analysis of spontaneous reporting system in Southern Italy. Drugs-Real World Outcomes 2020, 7, 41–51.
58. Singer JZ; Wallace SL The allopurinol hypersensitivity syndrome. Unnecessary morbidity and mortality. Arthritis Rheum 1986, 29, 82–87. [PubMed: 3947418]
59. Raper R; Ibels L; Lauer C; Barnes P; Lunzer M Fulminant hepatic failure due to allopurinol. Aust. N.Z. J. Med 1984, 14, 63–65. [PubMed: 6590011]
60. Rodevand E; Sletvold O; Kvande KT Side effects off allopurinol. Tidsskr. Nor. Legeforen 2004, 124, 2618–2619.
61. Mackenzie IS; Ford I; Nuki G; Hallas J; Hawkey CJ; Webster J; Ralston SH; Walters M; Robertson M; De Caterina R Long-term cardiovascular safety of febuxostat compared with allopurinol in patients with gout (FAST): a multicentre, prospective, randomised, open-label, non-inferiority trial. Lancet 2020, 396, 1745–1757. [PubMed: 33181081]

62. Hille R; Massey V Tight binding inhibitors of xanthine oxidase. Pharmacol. Ther 1981, 14, 249–263. [PubMed: 6895556]

63. Hawkes TR; George GN; Bray R The structure of the inhibitory complex of alloxanthine (1 H-pyrazolo [3, 4-d] pyrimidine-4, 6-diol) with the molybdenum centre of xanthine oxidase from electron-paramagnetic-resonance spectroscopy. Biochem. J 1984, 218, 961–968. [PubMed: 6326752]

64. Wortmann R; Ridolfo A; Lightfoot R Jr.; Fox I Antihyperuricemic properties of amflutizole in gout. J. Rheumatol 1985, 12, 540–543. [PubMed: 3900392]

65. Skibo EB Noncompetitive and irreversible inhibition of xanthine oxidase by benzimidazole analogs acting at the functional flavin adenine dinucleotide cofactor. Biochemistry 1986, 25, 4189–4194. [PubMed: 3756135]

66. Sato S; Tatsumi K; Nishino T A novel xanthine dehydrogenase inhibitor (BOF-4272). In Purine and pyrimidine metabolism in man VII; Springer, 1991, pp 135–138.

67. Okamoto K; Nishino T Mechanism of Inhibition of Xanthine Oxidase with a New Tight Binding Inhibitor (∗). J. Biol. Chem 1995, 270, 7816–7821. [PubMed: 7713871]

68. Nagamatsu T; Yamasaki H; Fujita T; Endo K; Machida H Novel xanthine oxidase inhibitor studies. Part 2. Synthesis and xanthine oxidase inhibitory activities of 2-substituted 6-alkylidenehydrazino- or 6-arylmethylidenehydrazino-7H-purines and 3-and/or 5-substituted 9H-1, 2, 4-triazolo [3, 4-i] purines. J. Chem. Soc., Perkin Trans 1 1999, 3117–3125.

69. Okamoto K; Eger BT; Nishino T; Kondo S; Pai EF; Nishino T An extremely potent inhibitor of xanthine oxidoreductase: crystal structure of the enzyme-inhibitor complex and mechanism of inhibition. J. Biol. Chem 2003, 278, 1848–1855. [PubMed: 12421831]

70. Okamoto K; Matsumoto K; Hille R; Eger BT; Pai EF; Nishino T The crystal structure of xanthine oxidoreductase during catalysis: implications for reaction mechanism and enzyme inhibition. Proc. Natl. Acad. Sci. U. S. A 2004, 101, 7931–7936. [PubMed: 15148401]

71. Fukunari A; Okamoto K; Nishino T; Eger BT; Pai EF; Kamezawa M; Yamada I; Kato N Y-700 [1-[3-Cyano-4-(2, 2-dimethylpropoxy) phenyl]-1H-pyrazole-4-carboxylic acid]: a potent xanthine oxidoreductase inhibitor with hepatic excretion. J. Pharmacol. Exp. Ther 2004, 311, 519–528. [PubMed: 15190124]

72. Tamta H; Thilagavathi R; Chakraborti AK; Mukhopadhyay AK 6-(N-benzoylamino) purine as a novel and potent inhibitor of xanthine oxidase: inhibition mechanism and molecular modeling studies. J. Enzyme Inhib. Med. Chem 2005, 20, 317–324. [PubMed: 16206825]

73. Pacher P; Nivorozhkin A; Szabo C Therapeutic effects of xanthine oxidase inhibitors: renaissance half a century after the discovery of allopurinol. Pharmacol. Rev 2006, 58, 87–114. [PubMed: 16507884]

74. Matsumoto K; Okamoto K; Ashizawa N; Nishino T FYX-051: a novel and potent hybrid-type inhibitor of xanthine oxidoreductase. J. Pharmacol. Exp. Ther 2011, 336, 95–103. [PubMed: 20952484]

75. Kumar R; Darpan; Sharma S; Singh R Xanthine oxidase inhibitors: a patent survey. Expert Opin. Ther. Pat 2011, 21, 1071–1108. [PubMed: 21510722]

76. Uematsu T; Nakashima M Pharmacokinetic and pharmacodynamics properties of a novel xanthine oxidase inhibitor, BOF-4272, in healthy volunteers. J. Pharmacol. Exp. Ther 1994, 270, 453–459. [PubMed: 8071837]

77. Komoriya K; Osada Y; Hasegawa M; Horiuchi H; Kondo S; Couch RC; Griffin TB Hypouricemic effect of allopurinol and the novel xanthine oxidase inhibitor TEI-6720 in chimpanzees. Eur. J. Pharmacol 1993, 250, 455–460. [PubMed: 8112406]

78. Osada Y; Tsuchimoto M; Fukushima H; Takahashi K; Kondo S; Hasegawa M; Komoriya K Hypouricemic effect of the novel xanthine oxidase inhibitor, TEI-6720, in rodents. Eur. J. Pharmacol 1993, 241, 183–188. [PubMed: 8243554]

79. Becker MA; Schumacher HR Jr.; Wortmann RL; MacDonald PA; Eustace D; Palo WA; Streit J; Joseph-Ridge N Febuxostat compared with allopurinol in patients with hyperuricemia and gout. N. Engl. J. Med 2005, 353, 2450–2461. [PubMed: 16339094]

80. Yamada I; Fukunari A; Osajima T; Kamezawa M; Mori H; Iwane J Pharmacokinetics/pharmacodynamics of Y-700, a novel xanthine oxidase inhibitor, in rats and man. Nucleosides, Nucleotides Nucleic Acids 2004, 23, 1123–1125. [PubMed: 15571214]

81. Hashimoto T; Fukunari A; Yamada I; Yanaka N; Chen D; Kato N Y-700, a novel inhibitor of xanthine oxidase, suppresses the development of colon aberrant crypt foci and cell proliferation in 1, 2-dimethylhydrazine-treated mice. Biosci., Biotechnol., Biochem 2005, 69, 209–211. [PubMed: 15665488]

82. Shimo T; Ashizawa N; Moto M; Matsumoto K; Iwanaga T; Nagata O FYX-051, a xanthine oxidoreductase inhibitor, induces nephropathy in rats, but not in monkeys. Toxicol. Pathol 2009, 37, 438–445. [PubMed: 19336671]

83. Hosoya T; Ishikawa T; Ogawa Y; Sakamoto R; Ohashi T Multicenter, open-label study of long-term topiroxostat (FYX-051) administration in Japanese hyperuricemic patients with or without gout. Clin. Drug Investig 2018, 38, 1135–1143.

84. Sato T; Ashizawa N; Matsumoto K; Iwanaga T; Nakamura H; Inoue T; Nagata O Discovery of 3-(3-cyano-4-pyridyl)-5-(4-pyridyl)-1, 2, 4-triazole, FYX-051-a xanthine oxidoreductase inhibitor for the treatment of hyperuricemia. Bioorg. Med. Chem. Lett 2009, 19, 6225–6229. [PubMed: 19783139]

85. Chen C; Lü J-M; Yao Q Hyperuricemia-related diseases and xanthine oxidoreductase (XOR) inhibitors: an overview. Med. Sci. Monit 2016, 22, 2501. [PubMed: 27423335]

86. Ojha R; Singh J; Ojha A; Singh H; Sharma S; Nepali K An updated patent review: xanthine oxidase inhibitors for the treatment of hyperuricemia and gout (2011–2015). Expert Opin. Ther. Pat 2017, 27, 311–345. [PubMed: 27841045]

87. Huneycutt E; Board C; Clements JN Lesinurad, a selective URAT-1 inhibitor with a novel mechanism in combination with a xanthine oxidase inhibitor, for hyperuricemia associated with gout. J. Pharm. Pract 2018, 31, 670–677.

88. Masuoka N; Kubo I Characterization of the xanthine oxidase inhibitory activity of alk (en) yl phenols and related compounds. Phytochemistry 2018, 155, 100–106. [PubMed: 30096514]

89. Kumar R; Joshi G; Kler H; Kalra S; Kaur M; Arya R Toward an understanding of structural insights of xanthine and aldehyde oxidases: an overview of their inhibitors and role in various diseases. Med. Res. Rev 2018, 38, 1073–1125. [PubMed: 28672082]

90. Mehmood A; Ishaq M; Zhao L; Safdar B; Rehman AU; Munir M; Raza A; Nadeem M; Iqbal W; Wang C Natural compounds with xanthine oxidase inhibitory activity: A review. Chem. Biol. Drug Des 2019, 93, 387–418. [PubMed: 30403440]

91. Malik N; Dhiman P; Khatkar A In silico and 3D QSAR studies of natural based derivatives as xanthine oxidase inhibitors. Curr. Top. Med. Chem 2019, 19, 123–138. [PubMed: 30727896]

92. Luna G; Dolzhenko AV; Mancera RL Inhibitors of Xanthine Oxidase: Scaffold Diversity and Structure-Based Drug Design. ChemMedChem 2019, 14, 714–743. [PubMed: 30740924]

93. Gunduğdu Ö; Noma SAA; Taskin-Tok T; Ateş B; Kishali N Evaluation of xanthine oxidase inhibitor properties on isoindoline-1, 3-dion derivatives and calculation of interaction mechanism. J. Mol. Struct 2020, 1204, No. 127523.

94. Chen LX; Schumacher HR Gout: an evidence-based review. J. Clin. Rheumatol 2008, 14, S55–S62. [PubMed: 18830092]

95. Richette P; Bardin T Gout. Lancet 2010, 375, 318–328. [PubMed: 19692116]

96. Vos T; Barber RM; Bell B; Bertozzi-Villa A; Biryukov S; Bolliger I; Charlson F; Davis A; Degenhardt L; Dicker D; Duan L; Erskine H; Feigin VL; Ferrari AJ; Fitzmaurice C; Fleming T; Graetz N; Guinovart C; Haagsma J; Hansen GM; Hanson SW; Heuton KR; Higashi H; Kassebaum N; Kyu H; Laurie E; Liang X; Lofgren K; Lozano R; MacIntyre MF; Moradi-Lakeh M; Naghavi M; Nguyen G; Odell S; Ortblad K; Roberts DA; Roth GA; Sandar L; Serina PT; Stanaway JD; Steiner C; Thomas B; Vollset SE; Whiteford H; Wolock TM; Ye P; Zhou M; Ãvila MA; Aasvang GM; Abbafati C; Ozgoren AA; Abd-Allah F; Aziz MIA; Abera SF; Aboyans V; Abraham JP; Abraham B; Abubakar I; Abu-Raddad LJ; Abu-Rmeileh NME; Aburto TC; Achoki T; Ackerman IN; Adelekan A; Ademi Z; Adou AK; Adsuar JC; Arnlov J; Agardh EE; al Khabouri MJ; Alam SS; Alasfoor D; Albittar MI; Alegretti MA; Aleman AV; Alemu ZA; Alfonso-Cristancho R; Alhabib S; Ali R; Alla F; Allebeck P; Allen PJ; AlMazroa MAA; Alsharif U; Alvarez E;

Alvis-Guzman N; Ameli O; Amini H; Ammar W; Anderson BO; Anderson HR; Antonio CAT; Anwari P; Apfel H; Arsenijevic VSA; Artaman A; Asghar RJ; Assadi R; Atkins LS; Atkinson C; Badawi A; Bahit MC; Bakfalouni T; Balakrishnan K; Balalla S; Banerjee A; Barker-Collo SL; Barquera S; Barregard L; Barrero LH; Basu S; Basu A; Baxter A; Beardsley J; Bedi N; Beghi E; Bekele T; Bell ML; Benjet C; Bennett DA; Bensenor IM; Benzian H; Bernabe E; Beyene TJ; Bhala N; Bhalla A; Bhutta Z; Bienhoff K; Bikbov B; Abdulhak AB; Blore JD; Blyth FM; Bohensky MA; Basara BB; Borges G; Bornstein NM; Bose D; Boufous S; Bourne RR; Boyers LN; Brainin M; Brauer M; Brayne CEG; Brazinova A; Breitborde NJK; Brenner H; Briggs ADM; Brooks PM; Brown J; Brugha TS; Buchbinder R; Buckle GC; Bukhman G; Bulloch AG; Burch M; Burnett R; Cardenas R; Cabral NL; Nonato IRC; Campuzano JC; Carapetis JR; Carpenter DO; Caso V; Castaneda-Orjuela CA; Catala-Lopez F; Chadha VK; Chang JC; Chen H; Chen W; Chiang PP; Chimed-Ochir O; Chowdhury R; Christensen H; Christophi CA; Chugh SS; Cirillo M; Coggeshall M; Cohen A; Colistro V; Colquhoun SM; Contreras AG; Cooper LT; Cooper C; Cooperrider K; Coresh J; Cortinovis M; Criqui MH; Crump JA; Cuevas-Nasu L; Dandona R; Dandona L; Dansereau E; Dantes HG; Dargan PI; Davey G; Davitoiu DV; Dayama A; de la Cruz-Gongora V; de la Vega SF; de Leo D; del Pozo-Cruz B; Dellavalle RP; Deribe K; Derrett S; Des Jarlais DC; Dessalegn M; deVeber GA; Dharmaratne SD; Diaz-Torne C; Ding EL; Dokova K; Dorsey ER; Driscoll TR; Duber H; Durrani AM; Edmond KM; Ellenbogen RG; Endres M; Ermakov SP; Eshrati B; Esteghamati A; Estep K; Fahimi S; Farzadfar F; Fay DFJ; Felson DT; Fereshtehnejad SM; Fernandes JG; Ferri CP; Flaxman A; Foigt N; Foreman KJ; Fowkes FGR; Franklin RC; Furst T; Futran ND; Gabbe BJ; Gankpe FG; Garcia-Guerra FA; Geleijnse JM; Gessner BD; Gibney KB; Gillum RF; Ginawi IA; Giroud M; Giussani G; Goenka S; Goginashvili K; Gona P; de Cosio TG; Gosselin RA; Gotay CC; Goto A; Gouda HN; Guerrant R; Gugnani HC; Gunnell D; Gupta R; Gupta R; Gutierrez RA; Hafezi-Nejad N; Hagan H; Halasa Y; Hamadeh RR; Hamavid H; Hammami M; Hankey GJ; Hao Y; Harb HL; Haro JM; Havmoeller R; Hay RJ; Hay S; Hedayati MT; Pi IBH; Heydarpour P; Hijar M; Hoek HW; Hoffman HJ; Hornberger JC; Hosgood HD; Hossain M; Hotez PJ; Hoy DG; Hsairi M; Hu H; Hu G; Huang JJ; Huang C; Huiart L; Husseini A; Iannarone M; Iburg KM; Innos K; Inoue M; Jacobsen KH; Jassal SK; Jeemon P; Jensen PN; Jha V; Jiang G; Jiang Y; Jonas JB; Joseph J; Juel K; Kan H; Karch A; Karimkhani C; Karthikeyan G; Katz R; Kaul A; Kawakami N; Kazi DS; Kemp AH; Kengne AP; Khader YS; Khalifa SEAH; Khan EA; Khan G; Khang YH; Khonelidze I; Kieling C; Kim D; Kim S; Kimokoti RW; Kinfu Y; Kinge JM; Kissela BM; Kivipelto M; Knibbs L; Knudsen AK; Kokubo Y; Kosen S; Kramer A; Kravchenko M; Krishnamurthi RV; Krishnaswami S; Defo BK; Bicer BK; Kuipers EJ; Kulkarni VS; Kumar K; Kumar GA; Kwan GF; Lai T; Lalloo R; Lam H; Lan Q; Lansingh VC; Larson H; Larsson A; Lawrynowicz AEB; Leasher JL; Lee JT; Leigh J; Leung R; Levi M; Li B; Li Y; Li Y; liang J; Lim S; Lin HH; Lind M; Lindsay MP; Lipshultz SE; Liu S; Lloyd BK; Ohno SL; Logroscino G; Looker KJ; Lopez AD; Lopez-Olmedo N; Lortet-Tieulent J; Lotufo PA; Low N; Lucas RM; Lunevicius R; Lyons RA; Ma J; Ma S; Mackay MT; Majdan M; Malekzadeh R; Mapoma CC; Marcenes W; March LM; Margono C; Marks GB; Marzan MB; Masci JR; Mason-Jones AJ; Matzopoulos RG; Mayosi BM; Mazorodze TT; McGill NW; McGrath JJ; McKee M; McLain A; McMahon BJ; Meaney PA; Mehndiratta MM; Mejia-Rodriguez F; Mekonnen W; Melaku YA; Meltzer M; Memish ZA; Mensah G; Meretoja A; Mhimbira FA; Micha R; Miller TR; Mills EJ; Mitchell PB; Mock CN; Moffitt TE; Ibrahim NM; Mohammad KA; Mokdad AH; Mola GL; Monasta L; Montico M; Montine TJ; Moore AR; Moran AE; Morawska L; Mori R; Moschandreas J; Moturi WN; Moyer M; Mozaffarian D; Mueller UO; Mukaigawara M; Murdoch ME; Murray J; Murthy KS; Naghavi P; Nahas Z; Naheed A; Naidoo KS; Naldi L; Nand D; Nangia V; Narayan KMV; Nash D; Nejjari C; Neupane SP; Newman LM; Newton CR; Ng M; Ngalesoni FN; Nhung NT; Nisar MI; Nolte S; Norheim OF; Norman RE; Norrving B; Nyakarahuka L; Oh IH; Ohkubo T; Omer SB; Opio JN; Ortiz A; Pandian JD; Panelo CIA; Papachristou C; Park EK; Parry CD; Caicedo AJP; Patten SB; Paul VK; Pavlin BI; Pearce N; Pedraza LS; Pellegrini CA; Pereira DM; Perez-Ruiz FP; Perico N; Pervaiz A; Pesudovs K; Peterson CB; Petzold M; Phillips MR; Phillips D; Phillips B; Piel FB; Plass D; Poenaru D; Polanczyk GV; Polinder S; Pope CA; Popova S; Poulton RG; Pourmalek F; Prabhakaran D; Prasad NM; Qato D; Quistberg DA; Rafay A; Rahimi K; Rahimi-Movaghar V; Rahman S; Raju M; Rakovac I; Rana SM; Razavi H; Refaat A; Rehm J; Remuzzi G; Resnikoff S; Ribeiro AL; Riccio PM; Richardson L; Richardus JH; Riederer AM; Robinson M; Roca A; Rodriguez A; Rojas-Rueda D; Ronfani L; Rothenbacher D; Roy N; Ruhago GM; Sabin N; Sacco RL; Ksoreide K; Saha S; Sahathevan R; Sahraian MA; Sampson

U; Sanabria JR; Sanchez-Riera L; Santos IS; Satpathy M; Saunders JE; Sawhney M; Saylan MI; Scarborough P; Schoettker B; Schneider IJC; Schwebel DC; Scott JG; Seedat S; Sepanlou SG; Serdar B; Servan-Mori EE; Shackelford K; Shaheen A; Shahraz S; Levy TS; Shangguan S; She J; Sheikhbahaei S; Shepard DS; Shi P; Shibuya K; Shinohara Y; Shiri R; Shishani K; Shiue I; Shrime MG; Sigfusdottir ID; Silberberg DH; Simard EP; Sindi S; Singh JA; Singh L; Skirbekk V; Sliwa K; Soljak M; Soneji S; Soshnikov SS; Speyer P; Sposato LA; Sreeramareddy CT; Stoeckl H; Stathopoulou VK; Steckling N; Stein MB; Stein DJ; Steiner TJ; Stewart A; Stork E; Stovner LJ; Stroumpoulis K; Sturua L; Sunguya BF; Swaroop M; Sykes BL; Tabb KM; Takahashi K; Tan F; Tandon N; Tanne D; Tanner M; Tavakkoli M; Taylor HR; te Ao BJ; Temesgen AM; Have MT; Tenkorang EY; Terkawi AS; Theadom AM; Thomas E; Thorne-Lyman AL; Thrift AG; Tleyjeh IM; Tonelli M; Topouzis F; Towbin JA; Toyoshima H; Traebert J; Tran BX; Trasande L; Trillini M; Truelsen T; Trujillo U; Tsilimbaris M; Tuzcu EM; Ukwaja KN; Undurraga EA; Uzun SB; van Brakel WH; van de Vijver S; Dingenen RV; van Gool CH; Varakin YY; Vasankari TJ; Vavilala MS; Veerman LJ; Velasquez-Melendez G; Venketasubramanian N; Vijayakumar L; Villalpando S; Violante FS; Vlassov VV; Waller S; Wallin MT; Wan X; Wang L; Wang JL; Wang Y; Warouw TS; Weichenthal S; Weiderpass E; Weintraub RG; Werdecker A; Wessells KRR; Westerman R; Wilkinson JD; Williams HC; Williams TN; Woldeyohannes SM; Wolfe CDA; Wong JQ; Wong H; Woolf AD; Wright JL; Wurtz B; Xu G; Yang G; Yano Y; Yenesew MA; Yentur GK; Yip P; Yonemoto N; Yoon SJ; Younis M; Yu C; Kim KY; Zaki MES; Zhang Y; Zhao Z; Zhao Y; Zhu J; Zonies D; Zunt JR; Salomon JA; Murray CJL Global, regional, and national incidence, prevalence, and years lived with disability for 301 acute and chronic diseases and injuries in 188 countries, 1990−2013: a systematic analysis for the Global Burden of Disease Study 2013. Lancet 2015, 386, 743–800. [PubMed: 26063472]

97. Elion GB; Kovensky A; Hitchings GH; Metz E; Rundles RW Metabolic studies of allopurinol, an inhibitor of xanthine oxidase. Biochem. Pharmacol 1966, 15, 863–880. [PubMed: 5967902]
98. Spector T; Johns D 4-Hydroxypyrazolo (3, 4-d) pyrimidine as a substrate for xanthine oxidase: loss of conventional substrate activity with catalytic cycling of the enzyme. Biochem. Biophys. Res. Commun 1970, 38, 583–589. [PubMed: 5462699]
99. Edmondson D; Ballou D; Van Heuvelen A; Palmer G; Massey V Kinetic studies on the substrate reduction of xanthine oxidase. J. Biol. Chem 1973, 248, 6135–6144. [PubMed: 4353632]
100. Olson JS; Ballou DP; Palmer G; Massey V The mechanism of action of xanthine oxidase. J. Biol. Chem 1974, 249, 4363–4382. [PubMed: 4367215]
101. Spector T; Hall WW; Krenitsky TA Human and bovine xanthine oxidases: inhibition studies with oxipurinol. Biochem. Pharmacol 1986, 35, 3109–3114. [PubMed: 3755906]
102. Mondal MS; Mitra S Kinetics and thermodynamics of the molecular mechanism of the reductive half-reaction of xanthine oxidase. Biochemistry 1994, 33, 10305–10312. [PubMed: 8068667]
103. Stockert AL; Shinde SS; Anderson RF; Hille R The reaction mechanism of xanthine oxidase: evidence for two-electron chemistry rather than sequential one-electron steps. J. Am. Chem. Soc 2002, 124, 14554–14555. [PubMed: 12465963]
104. Choi E-Y; Stockert AL; Leimkühler S; Hille R Studies on the mechanism of action of xanthine oxidase. J. Inorg. Biochem 2004, 98, 841–848. [PubMed: 15134930]
105. Yamaguchi Y; Matsumura T; Ichida K; Okamoto K; Nishino T Human xanthine oxidase changes its substrate specificity to aldehyde oxidase type upon mutation of amino acid residues in the active site: roles of active site residues in binding and activation of purine substrate. J. Biochem 2007, 141, 513–524. [PubMed: 17301077]
106. Amano T; Ochi N; Sato H; Sakaki S Oxidation reaction by Xanthine oxidase. Theoretical study of reaction mechanism. J. Am. Chem. Soc 2007, 129, 8131–8138. [PubMed: 17564439]
107. Alfaro JF; Jones JP Studies on the mechanism of aldehyde oxidase and xanthine oxidase. J. Org. Chem 2008, 73, 9469–9472. [PubMed: 18998731]
108. Bayse CA Density-functional theory models of xanthine oxidoreductase activity: comparison of substrate tautomerization and protonation. Dalton Trans 2009, 2306-2314, 2306. [PubMed: 19290363]
109. Metz S; Thiel W A combined QM/MM study on the reductive half-reaction of xanthine oxidase: substrate orientation and mechanism. J. Am. Chem. Soc 2009, 131, 14885–14902. [PubMed: 19788181]

110. Metz S; Thiel W QM/MM studies of xanthine oxidase: variations of cofactor, substrate, and active-site Glu802. J. Phys. Chem. B 2010, 114, 1506–1517. [PubMed: 20050623]
111. Du Y; Liu Z; Qiao F; Wang S; Chen K; Zhang X Computational exploration of reactive fragment for mechanism-based inhibition of xanthine oxidase. J. Organomet. Chem 2018, 864, 58–67.
112. Ribeiro PM; Fernandes HS; Maia LB; Sousa SF; Moura JJ; Cerqueira NM The complete catalytic mechanism of xanthine oxidase: a computational study. Inorg. Chem. Front 2021, 8, 405–416.
113. Bray MR; Deeth RJ The catalytic activity of xanthine oxidase: mechanistic insights throughcomputer modelling. J. Chem. Soc., Dalton Trans 1997, 1267–1268.
114. Zhang X-H; Wu Y-D A theoretical study on the mechanism of the reductive half-reaction of xanthine oxidase. Inorg. Chem 2005, 44, 1466–1471. [PubMed: 15732988]
115. Ilich P; Hille R Mechanism of Formamide Hydroxylation Catalyzed by a Molybdenum−Dithiolene Complex: A Model for Xanthine Oxidase Reactivity. J. Phys. Chem. B 1999, 103, 5406–5412.
116. Maiti NC; Tomita T; Kitagawa T; Okamoto K; Nishino T Resonance Raman studies on xanthine oxidase: observation of MoVI-ligand vibrations. J. Biol. Inorg. Chem 2003, 8, 327–333. [PubMed: 12589568]
117. Schopfer LM; Massey V; Nishino T Rapid reaction studies on the reduction and oxidation of chicken liver xanthine dehydrogenase by the xanthine/urate and NAD/NADH couples. J. Biol. Chem 1988, 263, 13528–13538. [PubMed: 3166459]
118. Kobayashi K; Miki M; Okamoto K; Nishino T Electron transfer process in milk xanthine dehydrogenase as studied by pulse radiolysis. J. Biol. Chem 1993, 268, 24642–24646. [PubMed: 8227023]
119. Anderson RF; Hille R; Massey V The radical chemistry of milk xanthine oxidase as studied by radiation chemistry techniques. J. Biol. Chem 1986, 261, 15870–15876. [PubMed: 3782094]
120. Kirk ML; Berhane A Correlating C□ H Bond Cleavage with Molybdenum Reduction in Xanthine Oxidase. Chem. Biodiversity 2012, 9, 1756–1760.
121. Sempombe J; Stein B; Kirk ML Spectroscopic and Electronic Structure Studies Probing Covalency Contributions to C−H Bond Activation and Transition-State Stabilization in Xanthine Oxidase. Inorg. Chem. 2011, 50, 10919–10928. [PubMed: 21972782]
122. Maghsoud Y; Dong C; Cisneros GA Computational Characterization of the Inhibition Mechanism of Xanthine Oxidoreductase by Topiroxostat. ACS Catal 2023, 6023–6043. [PubMed: 37547543]
123. Okamoto K; Eger BT; Nishino T; Pai EF; Nishino T Mechanism of inhibition of xanthine oxidoreductase by allopurinol: crystal structure of reduced bovine milk xanthine oxidoreductase bound with oxipurinol. Nucleosides, Nucleotides Nucleic Acids 2008, 27, 888–893. [PubMed: 18600558]
124. Okamoto K; Kusano T; Nishino T Chemical nature and reaction mechanisms of the molybdenum cofactor of xanthine oxidoreductase. Curr. Pharm. Des 2013, 19, 2606–2614. [PubMed: 23116398]
125. Pearson A; Godber B; Eisenthal R; Taylor G; Harrison R Human milk xanthine dehydrogenase is incompletely converted to the oxidase form in the absence of proteolysis. A Structural Explanation, 2006.
126. Eswar N; Eramian D; Webb B; Shen M-Y; Sali A Protein structure modeling with MODELLER. In Structural proteomics; Springer, 2008; pp 145–159.
127. Eswar N; Webb B; Marti-Renom MA; Madhusudhan M; Eramian D; Shen MY; Pieper U; Sali A Comparative protein structure modeling using Modeller. Curr. Protoc. Bioinf 2006, 15, 5.61–5.6.32.
128. Moult J; Fidelis K; Kryshtafovych A; Schwede T; Tramontano A Critical assessment of methods of protein structure prediction (CASP)_round x. Proteins: Struct., Funct., Bioinf 2014, 82, 1–6.
129. Haas J; Roth S; Arnold K; Kiefer F; Schmidt T; Bordoli L; Schwede T The Protein Model Portal_a comprehensive resource for protein structure and model information. Database 2013, 2013, No. bat031. [PubMed: 23624946]
130. Ferreira P; Cerqueira NM; Bras NF; Fernandes PA; Ramos MJ Parametrization of Molybdenum Cofactors for the AMBER Force Field. J. Chem. Theory Comput 2018, 14, 2538–2548. [PubMed: 29630831]

131. Li P; Merz K Jr. MCPB. py: A Python Based Metal Center Parameter Builder. J. Chem. Inf. Model 2016, 56, 599–604. [PubMed: 26913476]

132. Bayly CI; Cieplak P; Cornell W; Kollman PA A wellbehaved electrostatic potential based method using charge restraints for deriving atomic charges: the RESP model. J. Phys. Chem 1993, 97, 10269–10280.

133. Dupradeau F-Y; Pigache A; Zaffran T; Savineau C; Lelong R; Grivel N; Lelong D; Rosanski W; Cieplak P; The RE Tools: Advances in RESP and ESP charge derivation and force field library building. Phys. Chem. Chem. Phys 2010, 12, 7821–7839. [PubMed: 20574571]

134. Vanquelef E; Simon S; Marquant G; Garcia E; Klimerak G; Delepine JC; Cieplak P; Dupradeau F-Y RED Server: a web service for deriving RESP and ESP charges and building force field libraries for new molecules and molecular fragments. Nucleic Acids Res 2011, 39, W511–W517. [PubMed: 21609950]

135. Wang J; Wolf RM; Caldwell JW; Kollman PA; Case DA Development and testing of a general amber force field. J. Comput. Chem 2004, 25, 1157–1174. [PubMed: 15116359]

136. Wang J; Wang W; Kollman PA; Case DA Automatic atom type and bond type perception in molecular mechanical calculations. J. Mol. Graphics Modell 2006, 25, 247–260.

137. Olsson MH; Sondergaard CR; Rostkowski M; Jensen JH PROPKA3: consistent treatment of internal and surface residues in empirical p K a predictions. J. Chem. Theory Comput 2011, 7, 525–537. [PubMed: 26596171]

138. Sondergaard CR; Olsson MH; Rostkowski M; Jensen JH Improved treatment of ligands and coupling effects in empirical calculation and rationalization of p K a values. J. Chem. Theory Comput 2011, 7, 2284–2295. [PubMed: 26606496]

139. Schafmeister C; Ross W; Romanovski V LEaP; University of California: San Francisco, 1995.

140. Case DA; Aktulga HM; Belfon K; Ben-Shalom I; Brozell SR; Cerutti DS; Cheatham TE III Cruzeiro VWD; Darden TA; Duke, R. E. Amber 2021; University of California: San Francisco, 2021.

141. Jorgensen WL; Chandrasekhar J; Madura JD; Impey RW; Klein ML Comparison of simple potential functions for simulating liquid water. J. Chem. Phys 1983, 79, 926–935.

142. Maier JA; Martinez C; Kasavajhala K; Wickstrom L; Hauser KE; Simmerling C ff14SB: improving the accuracy of protein side chain and backbone parameters from ff99SB. J. Chem. Theory Comput 2015, 11, 3696–3713. [PubMed: 26574453]

143. Salomon-Ferrer R; Gotz AW; Poole D; Le Grand S; Walker RC Routine microsecond molecular dynamics simulations with AMBER on GPUs. 2. Explicit solvent particle mesh Ewald. J. Chem. Theory Comput 2013, 9, 3878–3888. [PubMed: 26592383]

144. Berendsen HJ; Postma J; van Gunsteren WF; DiNola A; Haak JR Molecular dynamics with coupling to an external bath. J. Chem. Phys 1984, 81, 3684–3690.

145. Zwanzig R Nonlinear generalized Langevin equations. J. Stat. Phys 1973, 9, 215–220.

146. Loncharich RJ; Brooks BR; Pastor RW Langevin dynamics of peptides: The frictional dependence of isomerization rates of N-acetylalanyl-N′-methylamide. Biopolymers 1992, 32, 523–535. [PubMed: 1515543]

147. Gillespie DT The chemical Langevin equation. J. Chem. Phys 2000, 113, 297–306.

148. Davidchack RL; Handel R; Tretyakov M Langevin thermostat for rigid body dynamics. J. Chem. Phys 2009, 130, 234101. [PubMed: 19548705]

149. Essmann U; Perera L; Berkowitz ML; Darden T; Lee H; Pedersen LG A smooth particle mesh Ewald method. J. Chem. Phys 1995, 103, 8577–8593.

150. Ryckaert J-P; Ciccotti G; Berendsen HJ Numerical integration of the cartesian equations of motion of a system with constraints: molecular dynamics of n-alkanes. J. Comput. Phys 1977, 23, 327–341.

151. Roe DR; Cheatham TE III PTRAJ and CPPTRAJ: software for processing and analysis of molecular dynamics trajectory data. J. Chem. Theory Comput 2013, 9, 3084–3095. [PubMed: 26583988]

152. Bakan A; Meireles LM; Bahar I ProDy: protein dynamics inferred from theory and experiments. Bioinformatics 2011, 27, 1575–1577. [PubMed: 21471012]

153. Likas A; Vlassis N; Verbeek JJ The global k-means clustering algorithm. Pattern Recognit 2003, 36, 451–461.

154. Kollman PA; Massova I; Reyes C; Kuhn B; Huo S; Chong L; Lee M; Lee T; Duan Y; Wang W; Donini O; Cieplak P; Srinivasan J; Case DA; Cheatham TE Calculating structures and free energies of complex molecules: combining molecular mechanics and continuum models. Acc. Chem. Res 2000, 33, 889–897. [PubMed: 11123888]

155. Wang W; Donini O; Reyes CM; Kollman PA Biomolecular simulations: recent developments in force fields, simulations of enzyme catalysis, protein-ligand, protein-protein, and protein-nucleic acid noncovalent interactions. Annu. Rev. Biophys. Biomol. Struct 2001, 30, 211–243. [PubMed: 11340059]

156. Wang J; Hou T; Xu X Recent advances in free energy calculations with a combination of molecular mechanics and continuum models. Curr. Comput.-Aided Drug Des 2006, 2, 287–306.

157. Hou T; Wang J; Li Y; Wang W Assessing the performance of the MM/PBSA and MM/GBSA methods. 1. The accuracy of binding free energy calculations based on molecular dynamics simulations. J. Chem. Inf. Model 2011, 51, 69–82. [PubMed: 21117705]

158. Hou T; Wang J; Li Y; Wang W Assessing the performance of the molecular mechanics/Poisson Boltzmann surface area and molecular mechanics/generalized Born surface area methods. II. The accuracy of ranking poses generated from docking. J. Comput. Chem 2011, 32, 866–877. [PubMed: 20949517]

159. Muzzioli E; Del Rio A; Rastelli G Assessing Protein Kinase Selectivity with Molecular Dynamics and MM-PBSA Binding Free Energy Calculations. Chem. Biol. Drug Des 2011, 78, 252–259. [PubMed: 21585710]

160. Xu L; Li Y; Li L; Zhou S; Hou T Understanding microscopic binding of macrophage migration inhibitory factor with phenolic hydrazones by molecular docking, molecular dynamics simulations and free energy calculations. Mol. BioSyst 2012, 8, 2260–2273. [PubMed: 22739754]

161. Sun H; Duan L; Chen F; Liu H; Wang Z; Pan P; Zhu F; Zhang JZ; Hou T Assessing the performance of MM/PBSA and MM/GBSA methods. 7. Entropy effects on the performance of end-point binding free energy calculation approaches. Phys. Chem. Chem. Phys 2018, 20, 14450–14460. [PubMed: 29785435]

162. Chen J; Zhang S; Wang W; Sun H; Zhang Q; Liu X Binding of inhibitors to BACE1 affected by pH-dependent protonation: An exploration from multiple replica Gaussian accelerated molecular dynamics and MM-GBSA calculations. ACS Chem. Neurosci 2021, 12, 2591–2607. [PubMed: 34185514]

163. Ongaro A; Oselladore E; Memo M; Ribaudo G; Gianoncelli A Insight into the LFA-1/SARS-CoV-2 Orf7a complex by protein−protein docking, molecular dynamics, and MM-GBSA calculations. J. Chem. Inf. Model 2021, 61, 2780–2787. [PubMed: 34043356]

164. Tuccinardi T What is the current value of MM/PBSA and MM/GBSA methods in drug discovery? Expert Opin. Drug Discovery 2021, 16, 1233–1237.

165. Naseem-Khan S; Berger MB; Leddin EM; Maghsoud Y; Cisneros GA Impact of Remdesivir Incorporation along the Primer Strand on SARS-CoV-2 RNA-Dependent RNA Polymerase. J. Chem. Inf. Model 2022, 62, 2456–2465. [PubMed: 35435671]

166. Kratz EG; Walker AR; Lagardère L; Lipparini F; Piquemal JP; Andres Cisneros G LICHEM: A QM/MM program for simulations with multipolar and polarizable force fields. J. Comput. Chem 2016, 37, 1019–1029. [PubMed: 26781073]

167. Gokcan H; Vazquez-Montelongo EA; Cisneros GA LICHEM 1.1: recent improvements and new capabilities. J. Chem. Theory Comput 2019, 15, 3056–3065. [PubMed: 30908049]

168. Frisch MJ; Trucks GW; Schlegel HB; Scuseria GE; Robb MA; Cheeseman JR; Scalmani G; Barone V; Petersson GA; Nakatsuji H; Li X; Caricato M; Marenich AV; Bloino J; Janesko BG; Gomperts R; Mennucci B; Hratchian HP; Ortiz JV; Izmaylov AF; Sonnenberg JL; Williams-Young D; Ding F; Lipparini F; Egidi F; Goings J; Peng B; Petrone A; Henderson T; Ranasinghe D; Zakrzewski VG; Gao J; Rega N; Zheng G; Liang W; Hada M; Ehara M; Toyota K; Fukuda R; Hasegawa J; Ishida M; Nakajima T; Honda Y; Kitao O; Nakai H; Vreven T; Throssell K; Montgomery JA Jr; Peralta JE; Ogliaro F; Bearpark MJ; Heyd JJ; Brothers EN; Kudin KN; Staroverov VN; Keith TA; Kobayashi R; Normand J; Raghavachari K; Rendell AP; Burant JC;

Iyengar SS; Tomasi J; Cossi M; Millam JM; Klene M; Adamo C; Cammi R; Ochterski JW; Martin RL; Morokuma K; Farkas O; Foresman JB; Fox DJ Gaussian 16 Rev. C.01: Wallingford, CT, 2016.

169. Rackers JA; Wang Z; Lu C; Laury ML; Lagardère L;Schnieders MJ; Piquemal JP; Ren P; Ponder JW Tinker 8: software tools for molecular design. J. Chem. Theory Comput 2018, 14, 5273–5289. [PubMed: 30176213]
170. Weigend F; Ahlrichs R Balanced basis sets of split valence, triple zeta valence and quadruple zeta valence quality for H to Rn: Design and assessment of accuracy. Phys. Chem. Chem. Phys 2005, 7, 3297–3305. [PubMed: 16240044]
171. Andrae D; Haeussermann U; Dolg M; Stoll H; Preuss H Energy-adjustedab initio pseudopotentials for the second and third row transition elements. Theor. Chim. Acta 1990, 77, 123–141.
172. Maghsoud Y; Vazquez-Montelongo EA; Yang X; Liu C; Jing Z; Lee J; Harger M; Smith AK; Espinoza M; Guo H-F; Kurie JM; Dalby KN; Ren P; Cisneros GA Computational Investigation of a Series of Small Molecules as Potential Compounds for Lysyl Hydroxylase-2 (LH2) Inhibition. J. Chem. Inf. Model 2023, 63, 986–1001. [PubMed: 36779232]
173. Simon S; Duran M; Dannenberg J How does basis set superposition error change the potential surfaces for hydrogenbonded dimers? J. Chem. Phys 1996, 105, 11024–11031.
174. Galano A; Alvarez-Idaboy JR A new approach to counterpoise correction to BSSE. J. Comput. Chem 2006, 27, 1203–1210. [PubMed: 16752366]
175. Dzib E; Cabellos JL; Ortiz-Chi F; Pan S; Galano A; Merino G Eyringpy: A program for computing rate constants in the gas phase and in solution. Int. J. Quantum Chem 2019, 119, No. e25686.
176. Dzib IE; Quintal A; Ortiz-Chi F; Merino G Eyringpy 2.0; Cinvestav: Merida, Yucatan, 2021.
177. Eyring H The activated complex in chemical reactions. J. Chem. Phys 1935, 3, 107–115.
178. Evans MG; Polanyi M Some applications of the transition state method to the calculation of reaction velocities, especially in solution. Trans. Faraday Soc 1935, 31, 875–894.
179. Eckart C The penetration of a potential barrier by electrons. Phys. Rev 1930, 35, 1303.
180. Johnson ER; Keinan S; Mori-Sanchez P; Contreras-Garcia J; Cohen AJ; Yang W Revealing noncovalent interactions. J. Am. Chem. Soc 2010, 132, 6498–6506. [PubMed: 20394428]
181. Lu T; Chen F Multiwfn: a multifunctional wavefunction analyzer. J. Comput. Chem 2012, 33, 580–592. [PubMed: 22162017]
182. Becke AD; Edgecombe KE A simple measure of electron localization in atomic and molecular systems. J. Chem. Phys 1990, 92, 5397–5403.
183. Silvi B; Savin A Classification of chemical bonds based on topological analysis of electron localization functions. Nature 1994, 371, 683–686.
184. Yang S; Xu G-Y; Han J-P; Bing H; Dou H; Zhang X-G Nitrogen-doped porous carbon derived from dopamine-modified polypyrrole and its electrochemical capacitive behavior. Acta Phys.-Chim. Sin 2015, 31, 685–692.
185. Lu T; Chen F-W Meaning and functional form of the electron localization function. Acta Phys.-Chim. Sin 2011, 27, 2786–2792.
186. Humphrey W; Dalke A; Schulten K VMD: visual molecular dynamics. J. Mol. Graph 1996, 14, 33–38. [PubMed: 8744570]
187. Singh UC; Kollman PA An approach to computing electrostatic charges for molecules. J. Comput. Chem 1984, 5, 129–145.
188. Besler BH; Merz KM Jr.; Kollman PA Atomic charges derived from semiempirical methods. J. Comput. Chem 1990, 11, 431–439.
189. Maghsoud Y; Jayasinghe-Arachchige VM; Kumari P; Cisneros GA; Liu J Leveraging QM/MM and Molecular Dynamics Simulations to Decipher the Reaction Mechanism of the Cas9 HNH Domain to Investigate off-Target Effects, 2023.
190. Graham SE; Syeda F; Cisneros GA Computational prediction of residues involved in fidelity checking for DNA synthesis in DNA polymerase I. Biochemistry 2012, 51, 2569–2578. [PubMed: 22397306]

191. Dewage SW; Cisneros GA Computational analysis of ammonia transfer along two intramolecular tunnels in Staphylococcus aureus glutamine-dependent amidotransferase (GatCAB). J. Phys. Chem. B 2015, 119, 3669–3677. [PubMed: 25654336]
192. Walker AR; Cisneros GA Computational simulations of DNA polymerases: detailed insights on structure/function/mechanism from native proteins to cancer variants. Chem. Res. Toxicol 2017, 30, 1922–1935. [PubMed: 28877429]
193. Nagamatsu T; Fujita T; Endo K Novel xanthine oxidase inhibitor studies. Part 3. 1 Convenient and general syntheses of 3-substituted 7 H-pyrazolo [4, 3-e]-1, 2, 4-triazolo [4, 3-c] pyrimidin-5 (6 H)-ones as a new class of potential xanthine oxidase inhibitors. J. Chem. Soc., Perkin Trans 1 2000, 33–42.
194. Boudet N; Knochel P Chemo-and regioselective functionalization of uracil derivatives. Applications to the synthesis of oxypurinol and emivirine. Org. Lett 2006, 8, 3737–3740. [PubMed: 16898805]
195. Day RO; Graham GG; Hicks M; McLachlan AJ; Stocker SL; Williams KM Clinical pharmacokinetics and pharmacodynamics of allopurinol and oxypurinol. Clin. Pharmacokinet 2007, 46, 623–644. [PubMed: 17655371]
196. Singla P; Luxami V; Singh R; Tandon V; Paul K Novel pyrazolo [3, 4-d] pyrimidine with 4-(1H-benzimidazol-2-yl)-phenylamine as broad spectrum anticancer agents: Synthesis, cell based assay, topoisomerase inhibition, DNA intercalation and bovine serum albumin studies. Eur. J. Med. Chem 2017, 126, 24–35. [PubMed: 27744184]
197. El-Mekabaty A; Etman HA; Mosbah A; Fadda AA Synthesis, In Vitro Cytotoxicity and Bleomycin-Dependent DNA Damage Evaluation of Some Heterocyclic-Fused Pyrimidinone Derivatives. ChemistrySelect 2020, 5, 4856–4861.
198. Plouvier BMC; Choi LS L. Crystal salt of xanthine oxidase inhibitors. WO2006083687A1, 2006.
199. Chalmers R; Parker R; Simmonds H; Snedden W; Watts R The conversion of 4-hydroxypyrazolo-[3, 4-d] pyrimidine (allopurinol) into 4, 6-dihydroxypyrazolo [3, 4-d] pyrimidine (oxipurinol) in vivo in the absence of xanthine–oxygen oxidoreductase. Biochem. J 1969, 112, 527–532. [PubMed: 5801674]
200. Nelson DJ; Bugge CJ; Krasny HC; Elion GB Formation of nucleotides of [6-14C] allopurinol and [6-14C] oxipurinol in rat tissues and effects on uridine nucleotide pools. Biochem. Pharmacol 1973, 22, 2003–2022. [PubMed: 4353669]
201. Stevenson A; Silcock S; Scott J Absence of chromosome damage in human lymphocytes exposed to allopurinol and oxipurinol. Ann. Rheum. Dis 1976, 35, 143–147. [PubMed: 942270]
202. Spector T Inhibition of urate production by allopurinol. Biochem. Pharmacol 1977, 26, 355–358. [PubMed: 849329]
203. Williams JW; Bray R Kinetic and epr studies on the inhibition of xanthine oxidase by alloxanthine (1 H-pyrazolo [3, 4-d] pyrimidine-4, 6-diol). Biochem. J 1981, 195, 753–760. [PubMed: 6274312]
204. Shaw M; Parsons D Absorption and metabolism of allopurinol and oxypurinol by rat jejunum in vitro: effects on uric acid transport. Clin. Sci 1984, 66, 257–267.
205. Hernandez R; Orozco M; Luque FJ Tautomerism of xanthine and alloxanthine: A model for substrate recognition by xanthine oxidase. J. Comput.-Aided Mol. Des 1996, 10, 535–544. [PubMed: 9007687]
206. Bergmann F; Frank A; Neiman Z Studies on the chemical reactivity and the physical properties of allopurinol (pyrazolo [3, 4-d] pyrimidin-4-one) and related compounds. J. Chem. Soc., Perkin Trans. 1 1979, 1, 2795–2802.
207. Hanggi G; Schmalle H; Dubler EN (8)-coordinating allopurinol: structure of bis (allopurinol) triaqua (sulfato) copper (II) hydrate. Acta Crystallogr., Sect. C: Cryst. Struct. Commun 1991, 47, 1609–1614.
208. Prusiner P; Sundaralingam M Stereochemistry of nucleic acids and their constituents. XXIX. Crystal and molecular structure of allopurinol, a potent inhibitor of xanthine oxidase. Acta Crystallogr., Sect. B: Struct. Crystallogr. Cryst. Chem 1972, 28, 2148–2152.

209. Waheed SO; Varghese A; Chaturvedi SS; Karabencheva-Christova TG; Christov CZ How Human TET2 Enzyme Catalyzes the Oxidation of Unnatural Cytosine Modifications in Double-Stranded DNA. ACS Catal 2022, 12, 5327–5344. [PubMed: 36339349]

210. Chaturvedi SS; Jaber Sathik Rifayee SB; Waheed SO; Wildey J; Warner C; Schofield CJ; Karabencheva-Christova TG; Christov CZ Can Second Coordination Sphere and Long-Range Interactions Modulate Hydrogen Atom Transfer in a Non-Heme Fe (II)-Dependent Histone Demethylase? JACS Au 2022, 2, 2169–2186. [PubMed: 36186565]

211. Nishino T; Okamoto K Mechanistic insights into xanthine oxidoreductase from development studies of candidate drugs to treat hyperuricemia and gout. J. Biol. Inorg. Chem 2015, 20, 195–207. [PubMed: 25501928]

212. Spector T; Johns D Stoichiometric inhibition of reduced xanthine oxidase by hydroxypyrazolo [3, 4-d] pyrimidines. J. Biol. Chem 1970, 245, 5079–5085. [PubMed: 5506275]

213. Krenitsky TA; Spector T; Hall WW Xanthine oxidase from human liver: purification and characterization. Arch. Biochem. Biophys 1986, 247, 108–119. [PubMed: 3010873]

214. Pauff JM; Cao H; Hille R Substrate orientation and catalysis at the Molybdenum site in xanthine oxidase. J. Biol. Chem 2009, 284, 8760–8767. [PubMed: 19109252]

215. Ilich P; Hille R Tautomerization of the substrate heterocycle in the course of the reaction of xanthine oxidase. Inorg. Chim. Acta 1997, 263, 87–93.

216. Pauff JM; Hemann CF; Jünemann N; Leimkühler S; Hille R The role of arginine 310 in catalysis and substrate specificity in xanthine dehydrogenase from Rhodobacter capsulatus. J. Biol. Chem 2007, 282, 12785–12790. [PubMed: 17327224]

217. Leimkühler, S; Stockert AL; Igarashi K; Nishino T; Hille R The role of active site glutamate residues in catalysis of Rhodobacter capsulatus xanthine dehydrogenase. J. Biol. Chem 2004, 279, 40437–40444. [PubMed: 15265866]

218. Glatigny A; Hof P; Romão MJ; Huber R; Scazzocchio C Altered specificity mutations define residues essential for substrate positioning in xanthine dehydrogenase. J. Mol. Biol 1998, 278, 431–438. [PubMed: 9571062]

219. Stiburkova B; Krijt J; Vyletal P; Bartl J; Gerhatova E; Korinek M; Sebesta I Novel mutations in xanthine dehydrogenase/oxidase cause severe hypouricemia: biochemical and molecular genetic analysis in two Czech families with xanthinuria type I. Clin. Chim. Acta 2012, 413, 93–99. [PubMed: 21963464]

220. Xu T; Xie X; Zhang Z; Zhao N; Deng Y; Li P A novel mutation in xanthine dehydrogenase in a case with xanthinuria in Hunan province of China. Clin. Chim. Acta 2020, 504, 168–171. [PubMed: 32067994]

221. Kudo M; Moteki T; Sasaki T; Konno Y; Ujiie S; Onose A; Mizugaki M; Ishikawa M; Hiratsuka M Functional characterization of human xanthine oxidase allelic variants. Pharmacogenet. Genomics 2008, 18, 243–251. [PubMed: 18300946]

222. Ichida K; Amaya Y; Kamatani N; Nishino T; Hosoya T; Sakai O Identification of two mutations in human xanthine dehydrogenase gene responsible for classical type I xanthinuria. J. Clin. Invest 1997, 99, 2391–2397. [PubMed: 9153281]

223. Arikyants N; Sarkissian A; Hesse A; Eggermann T; Leumann E; Steinmann B Xanthinuria type I: a rare cause of urolithiasis. Pediatr. Nephrol 2007, 22, 310–314. [PubMed: 17115198]

224. Gok F; Ichida K; Topaloglu R Mutational analysis of the xanthine dehydrogenase gene in a Turkish family with autosomal recessive classical xanthinuria. Nephrol., Dial., Transplant 2003, 18, 2278–2283. [PubMed: 14551354]

225. Tanaka K-I; Kanazawa I; Yamasaki H; Hasegawa H; Ichida K; Sugimoto T Xanthinuria type I with a novel mutation of xanthine dehydrogenase. Am. J. Med. Sci 2015, 350, 155–156. [PubMed: 26110747]

226. Johns DG Anomalous differential effects of 4-hydroxypyrazolo (3, 4-d)-pyrimidine on electron transfer from xanthine oxidase to molecular oxygen and to acceptor dyes. Biochem. Biophys. Res. Commun 1968, 31, 197–202. [PubMed: 5656067]

227. Spector T; Johns D Oxidation of 4-hydroxypyrazolo (3, 4-d) pyrimidine by xanthine oxidase: The route of electron transfer from substrate to acceptor dyes. Biochem. Biophys. Res. Commun 1968, 32, 1039–1044. [PubMed: 5750222]

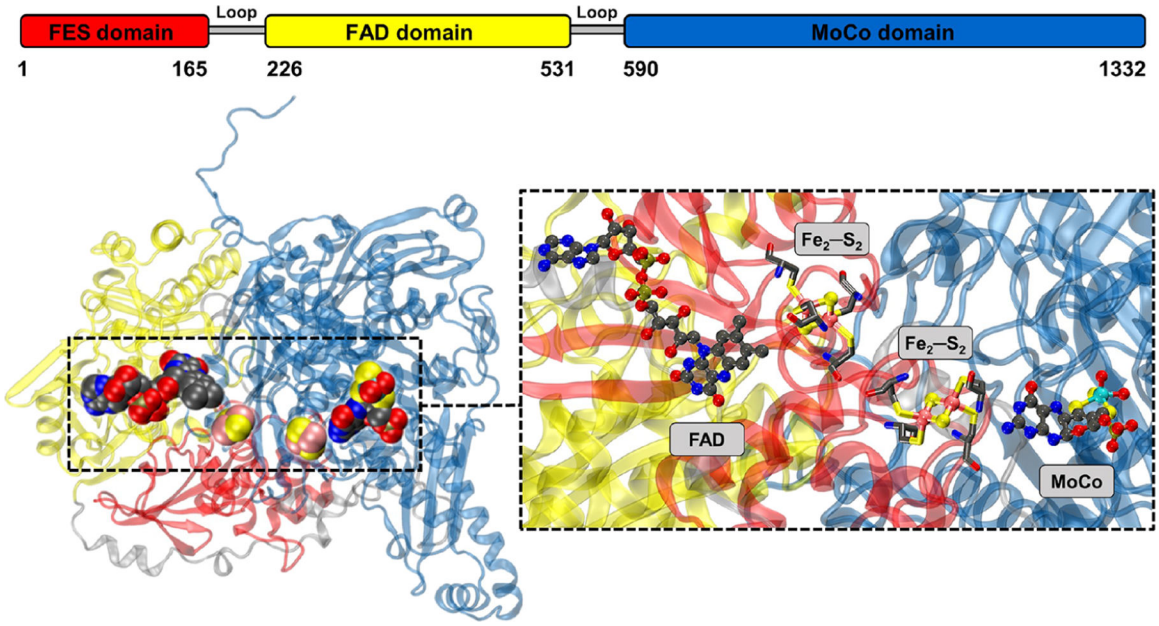

Figure 1.

One subunit of the bovine xanthine oxidoreductase homodimer (PDB ID: 1JRO).[47] The close-up represents the XOR's active regions in the redox reaction that are almost linearly positioned in the order of MoCo, $Fe_2 - S_2$, and FAD. Hydrogen atoms are not presented for more clarity, and four cysteine residues bound to the $Fe_2 - S_2$ cluster's irons are shown in the sticks.

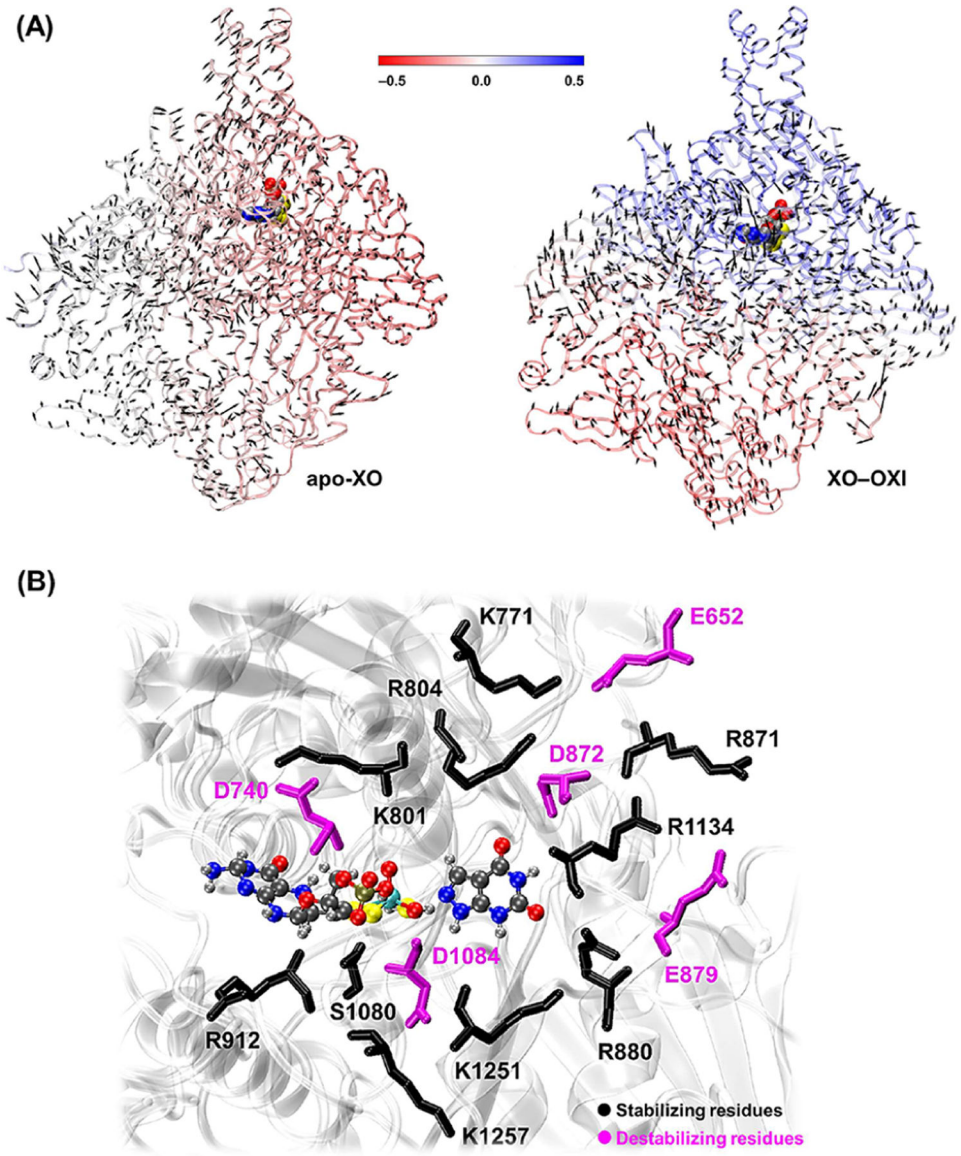

Figure 2.

(A) Plots of the PCA on the root-mean-square fluctuations (first mode) along with the residue-wise correlation with respect to MoCo as a heatmap projected on the protein for the apo-XO and XO–OXI. The black arrows show the fluctuations greater than 1.0 Å and point toward the direction of the highest ranked eigenvector, and their amplitude is directly proportional to the length of the arrow. Areas with correlated movements in the heatmap are colored blue (0.5), non-correlated areas are white (0.0), and anti-correlated movements are red (−0.5). (B) Representation of the residues with considerable non-bonded intermolecular interactions ($||\Delta E_{NB}| \geq 12.0$ kcal mol^{-1}) with the MoCo of XO–OXI compared to that of the apo-XO as the reference.

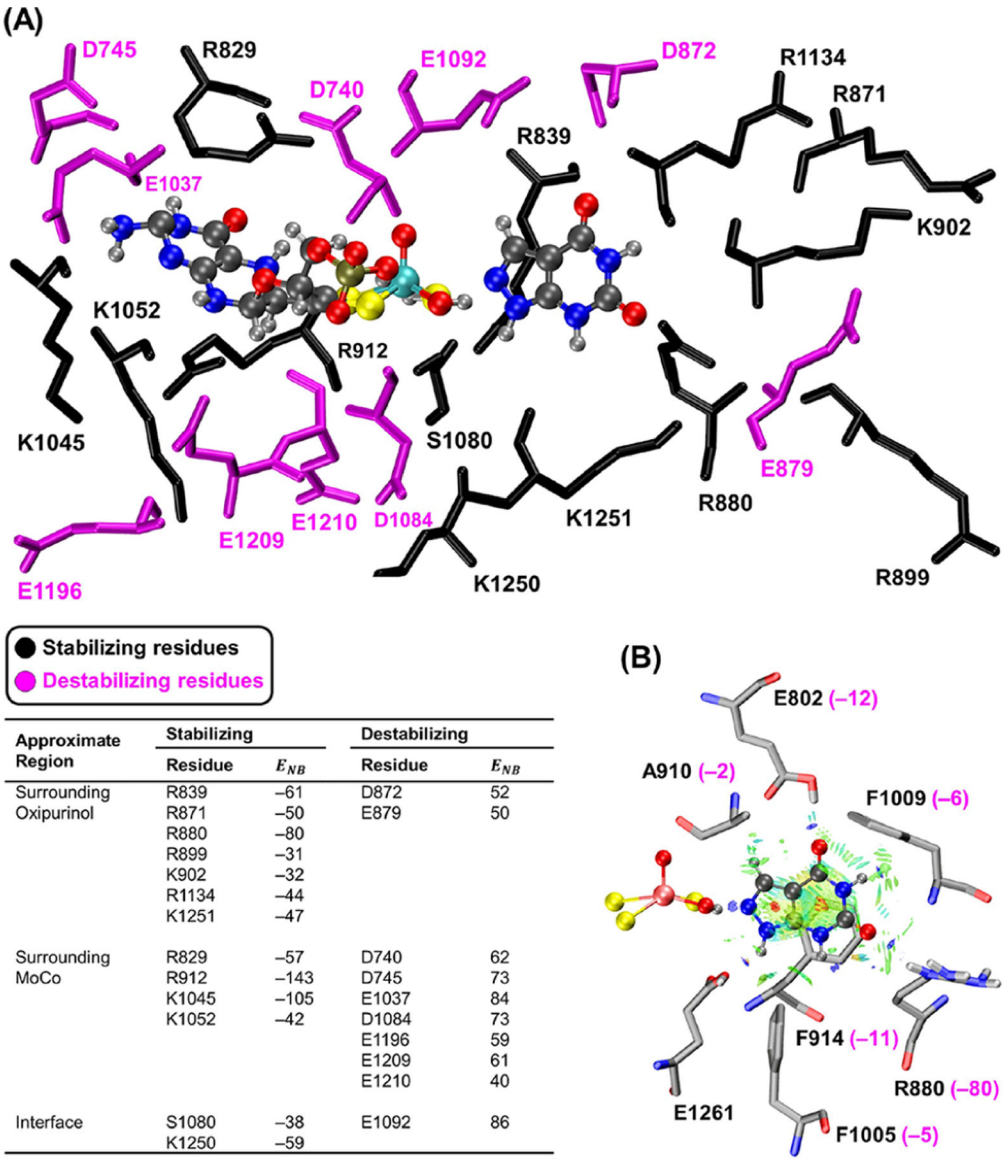

Approximate Region	Stabilizing		Destabilizing	
	Residue	E_{NB}	Residue	E_{NB}
Surrounding Oxipurinol	R839	–61	D872	52
	R871	–50	E879	50
	R880	–80		
	R899	–31		
	K902	–32		
	R1134	–44		
	K1251	–47		
Surrounding MoCo	R829	–57	D740	62
	R912	–143	D745	73
	K1045	–105	E1037	84
	K1052	–42	D1084	73
			E1196	59
			E1209	61
			E1210	40
Interface	S1080	–38	E1092	86
	K1250	–59		

Figure 3.

(A) Residues of the XO–OXI active site with considerable non-bonded intermolecular interactions ($|E_{NB}| \geq 30$ kcal mol^{-1}). Residues in the sticks have stabilizing (black) and destabilizing (purple) interactions with the active site, given in the ball-and-sticks. E1261 of the active site is not shown for enhanced clarity. (B) Plot of the aNCI between the inhibitor and the surrounding residues of the active site. Values in parenthesis correspond to E_{NB} (kcal mol^{-1}) of each residue.

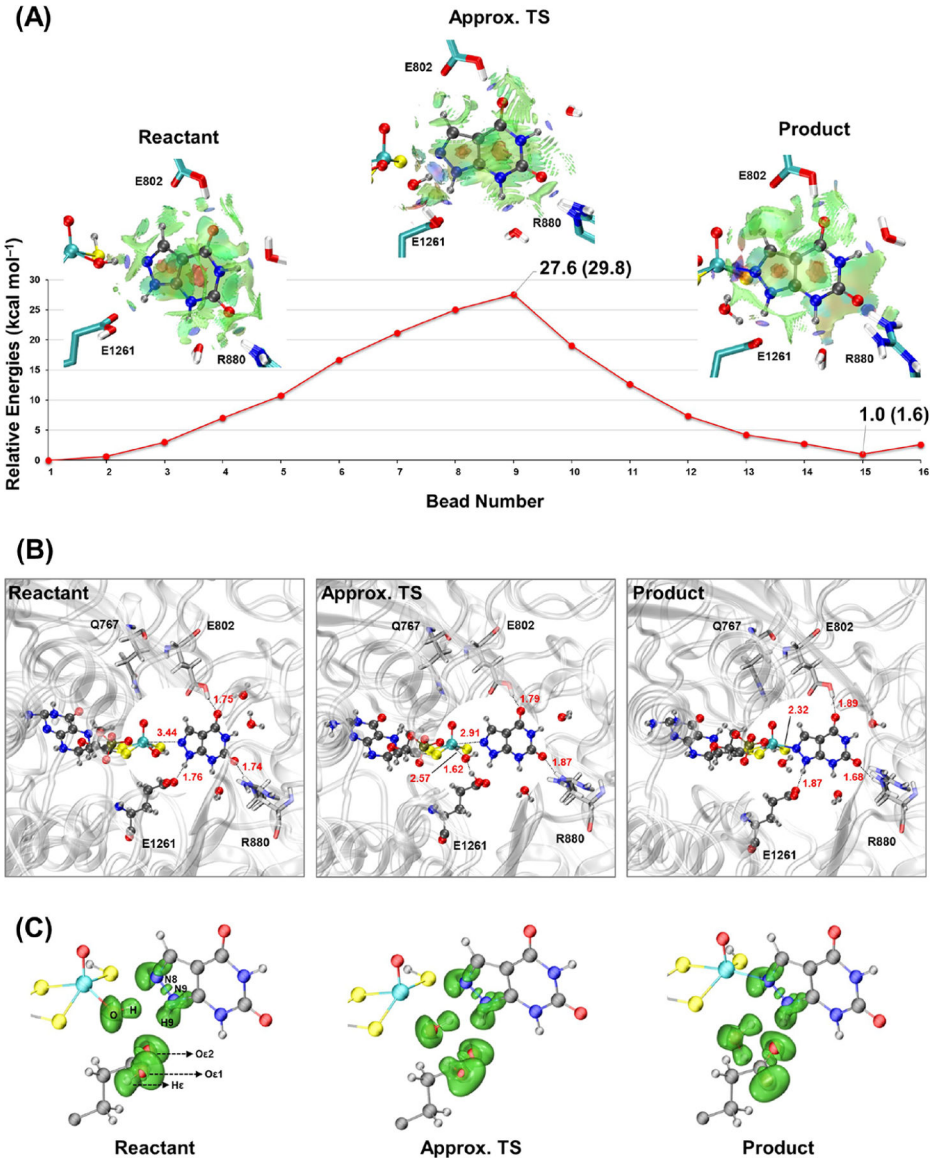

Figure 4.

(A) Minimum energy path for the catalytic inhibition of XO by oxipurinol modeled via the QSM together with the NCI plots of the critical structures. The QM/MM optimization energies (kcal mol^{-1}) are calculated at the ω B97X-D/def2-SVP level of theory with the AMBER ff14SB force field. The values in parenthesis correspond to the Gibbs free energies obtained from the vibrational analysis using Eyringpy. (B) Optimized geometries of the critical structures with the values of selected distances (Å). (C) ELF basins among the MoCo, oxipurinol, and E1261 for the critical structures along the reaction pathway.

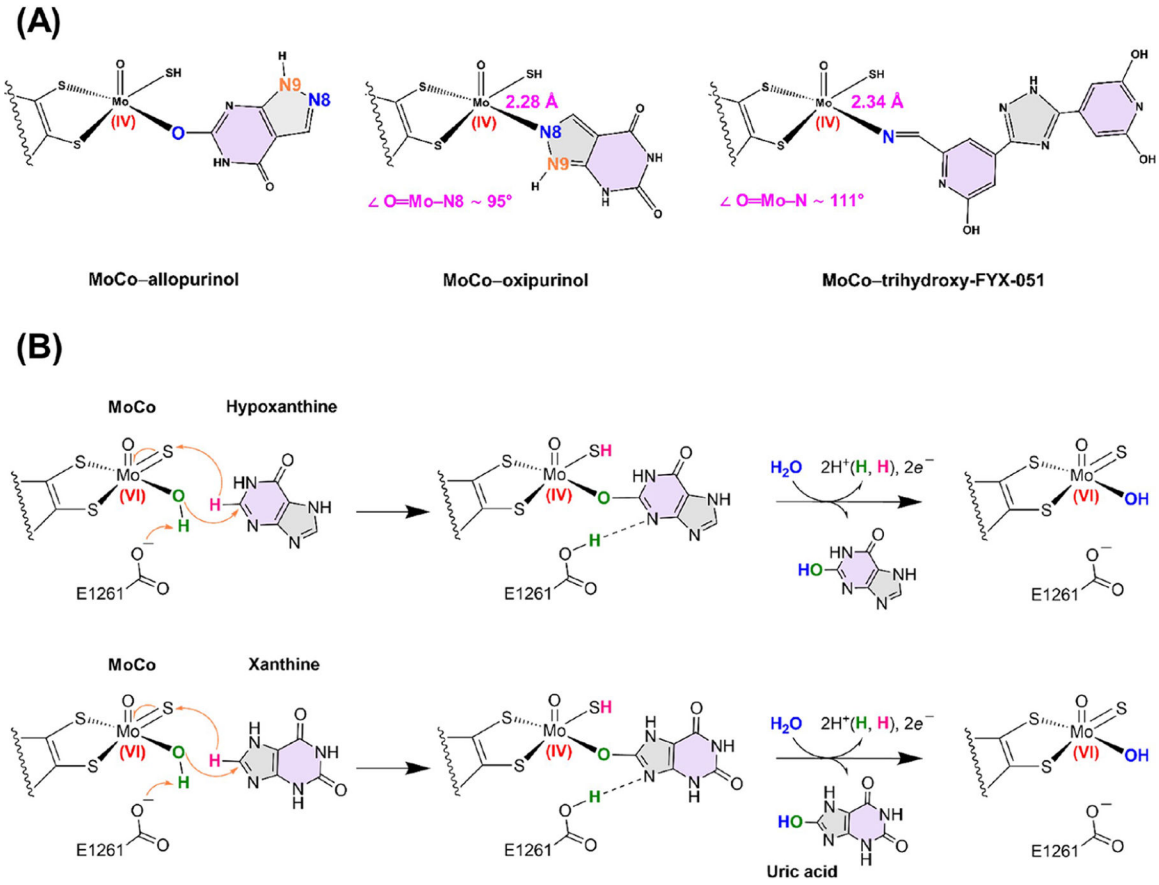

Scheme 1.

(A) Coordination Modes in Left: MoCo–Allopurinol; Middle: MoCo–Oxipurinol with a Direct Mo–N8 Bond (PDB IDs: 1JRP & 3BDJ);[47,123] and Right: MoCo–Trihydroxy-FYX-051 with a Mo–N≡C Bond (PDB ID: 3AM9);[74] (B) Proposed Reaction Mechanisms for the Hydroxylation of Hypoxanthine and Xanthine in the Active Site of XOR.

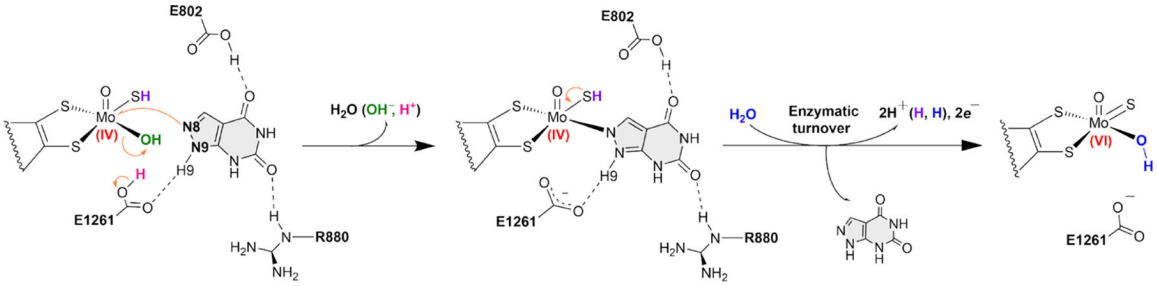

Scheme 2.

Studied Mechanism for the Catalytic Inhibition of XO by Oxipurinol